NAVAL POSTGRADUATE SCHOOL
Monterey, California

DTIC
ELECTE
JUN 1 8 1982
S   D
F

THESIS

AERODYNAMIC LOADS ON A BALL-OBTURATED
TUBULAR PROJECTILE

by

William Arthur Bry

March 1982

Thesis Advisor: R. H. Nunn

Approved for public release, distribution unlimited.

REPORT DOCUMENTATION PAGE		READ INSTRUCTIONS BEFORE COMPLETING FORM
1. REPORT NUMBER	2. GOVT ACCESSION NO. AD-A115756	3. RECIPIENT'S CATALOG NUMBER
4. TITLE (and Subtitle) Aerodynamic Loads on a Ball-Obturated Tubular Projectile		5. TYPE OF REPORT & PERIOD COVERED Master's Thesis March 1982
		6. PERFORMING ORG. REPORT NUMBER
7. AUTHOR(s) William Arthur Bry		8. CONTRACT OR GRANT NUMBER(s)
9. PERFORMING ORGANIZATION NAME AND ADDRESS Naval Postgraduate School Monterey, California 93940		10. PROGRAM ELEMENT, PROJECT, TASK AREA & WORK UNIT NUMBERS
11. CONTROLLING OFFICE NAME AND ADDRESS Naval Postgraduate School Monterey, California 93940		12. REPORT DATE March 1982
		13. NUMBER OF PAGES 68
14. MONITORING AGENCY NAME & ADDRESS(if different from Controlling Office)		15. SECURITY CLASS. (of this report) Unclasssified
		15a. DECLASSIFICATION/DOWNGRADING SCHEDULE

16. DISTRIBUTION STATEMENT (of this Report)

Approved for public release; distribution unlimited.

17. DISTRIBUTION STATEMENT (of the abstract entered in Block 20, if different from Report)

18. SUPPLEMENTARY NOTES

19. KEY WORDS (Continue on reverse side if necessary and identify by block number)

Tubular Projectile
Hollow Projectile
Developmental Ammunition

20. ABSTRACT (Continue on reverse side if necessary and identify by block number)

A tubular projectile is one with a hole bored along its longitudinal axis. The hole presents a problem in getting the round expelled from a gun. Some means of sealing the hole until the round clears the muzzle is required. A ball-obturator offers one practical means of accomplishing this without any accompanying FOD hazard. The ball-obturator, analogous to a common ball-valve, remains closed under the force of the expanding propellant charge and opens as soon as it is released. The high projectile

DD FORM 1473 EDITION OF 1 NOV 68 IS OBSOLETE
1 JAN 73
S/N 0102-014-6601

spin rate created in the barrel causes the ball to align its ports with the projectile tube through a complex gyrodynamic motion that is highly dependent upon the external moments relative to the spinning projectile.

This study presents results of wind-tunnel tests designed to quantify lift, drag, and moment forces imparted to the projectile by the ball as it transitions to a full open position. Wind-tunnel balance designs are discussed and equations for deduction of forces are presented. Drag and moment coefficients are plotted as functions of ball angle and presented along with Schlieren photographs of the flow at each test point. Techniques for separating tunnel interference from projectile forces are presented along with an uncertainty analysis.

Consistent results are obtained for drag measurement. Lift forces proved undeterminable with the balance design used. Moment measurements showed much data scatter though interesting trends are noted and correlations made with the flow visualizations. Finally the balance deficiencies are uncovered through the uncertainty analysis and a new design is proposed for increasing the accuracy of the moment measurement.

Accession For

NTIS GRA&I ☒
DTIC TAB ☐
Unannounced ☐
Justification

By
Distribution/
Availability Codes

Dist	Avail and/or Special
A	

DTIC COPY INSPECTED 2

Aerodynamic Loads on a Ball-Obturated
Tubular Projectile

by

William Arthur Bry
Lieutenant, United States Navy
B.S., Wofford College, 1974

Submitted in partial fulfillment of the
requirements for the degree of

MASTER OF SCIENCE IN MECHANICAL ENGINEERING

from the

NAVAL POSTGRADUATE SCHOOL
March 1982

Author _____

Approved by: _____
                                        Thesis Advisor

            _____
                                        Second Reader

            _____
            Chairman, Department of Mechanical Engineering

            _____
                        Dean of Science and Engineering

3

ABSTRACT

A tubular projectile is one with a hole bored along its longitudinal axis. The hole presents a problem in getting the round expelled from a gun. Some means of sealing the hole until the round clears the muzzle is required. A ball-obturator offers one practical means of accomplishing this without any accompanying FOD hazard. The ball-obturator, analogous to a common ball-valve, remains closed under the force of the expanding propellant charge and opens as soon as it is released. The high projectile spin rate ated in the barrel causes the ball to align its ports with the projectile tube through a complex gyrodynamic motion that is highly dependent upon the external moments relative to the spinning projectile.

This study presents results of wind-tunnel tests designed to quantify lift, drag, and moment forces imparted to the projectile by the ball as it transitions to a full open position. Wind-tunnel balance designs are discussed and equations for deduction of forces are presented. Drag and moment coefficients are plotted as functions of ball angle and presented along with Schlieren photographs of the flow at each test point. Techniques for separating tunnel interference from projectile forces are presented along with an uncertainty analysis.

Consistent results are obtained for drag measurement. Lift forces proved undeterminable with the balance design used. Moment

measurements showed much data scatter though interesting trends are noted and correlations made with the flow visualizations. Finally the balance deficiencies are uncovered through the uncertainty analysis and a new design is proposed for increasing the accuracy of the moment measurement.

TABLE OF CONTENTS

7

LIST OF TABLES

LIST OF FIGURES

TABLE OF SYMBOLS

$$C_D = \frac{D}{1/2 \ P_W \ M_\infty^2 kS}$$

C_D = projectile drag coefficient

$C_{D_{PR}}$ = reference projectile drag coefficient

C_{D_T} = total measured drag coefficient

$C_{D_{TA}}$ = interference drag coefficient

$C_{D_{TH}}$ = theoretical interference drag coefficient

$C_{D_{TS}}$ = total measured drag coefficient for a reference projectile

$$C_M = \frac{M}{1/2 \ P_W \ M_\infty^2 kSd}$$

C_M = projectile moment coefficient

C_{M_T} = total measured moment coefficient

$C_{M_{TA}}$ = interference moment coefficient

D = drag

d = nominal projectile diameter (19.939 mm)

D_S = strut drag

K = proportionality constant obtained from balance calibration and used in data reduction

k = ratio of specific heats (1.4 for air)

ℓ = moment-arm for measurements of overturning moments

M = moment

M_∞ = nominal Mach number

P_O = plenum pressure

P_w = test section static pressure

S = $\dfrac{\pi d^2}{4}$

Y = lift

$\overline{y}_\ell$ = distance from lower gage pair to measurement point at top of strut - a product of balance calibration

$\overline{y}_u$ = distance from upper gage pair to measurement point at top of strut - a product of balance calibration

α = angle of attack

θ = ball angle

I. INTRODUCTION

A. BACKGROUND

A tubular projectile is one with a hole bored down the longitudinal axis which allows free passage of air during flight. The advantages include a reduced effective frontal area which may contribute to a reduction in overall drag coefficient, C_D. A lower C_D results in higher projectile velocities at any given point downrange. Thus, if properly designed, a tubular projectile may have a shorter time of flight to the target and transfer more destructive kinetic energy on impact. Such results have been demonstrated during range tests conducted for concept evaluation of the 20-mm tubular projectile for the Vulcan System [1]. In these tests a tubular projectile was shown to have a time of flight that was 30 percent shorter at 1000 meters and 40 percent shorter at 2000 meters. Even though, in some cases, a tubular projectile may have less mass than a standard round, the kinetic energy delivered on target may be greater as it increases with the square of the velocity but only linearly with the mass. Other tests conducted by Rhethorst, et. al. [2] have shown that even with the same energy of impact the tubular projectile penetrates further. It has also been noted that the hole made by a tubular projectile will not close because a circular plug is cut from the target. Studies conducted by Kitchen and Keeser [3]

12

showed that 20-mm tubular projectiles penetrated simulated
aircraft fuel cells even when fired at angles up to 70 degrees
from the normal. Standard M56 HEI projectiles failed to breach
the same target at the higher degrees of obliquity although
severe damage did result.

The disadvantages to the tubular projectile include high
manufacturing costs, possible incompatibility with present
weapon systems, and less mass for a given caliber which may
negate the lower C_D advantage in larger guns. Even in the
small calibers the aerodynamic advantages have still not been
firmly established. In the report of a study conducted by
Charters and Thomas [4] at the Aberdeen Proving Ground it was
concluded that, "The aerodynamic performance of a tubular pro-
jectile can be equaled or bettered by a well streamlined,
solid projectile."

B. AN OBSTACLE TO PRACTICAL APPLICATION

One obvious problem associated with tubular projectiles
is blocking the hole while it is still in the gun to keep the
expanding propellant gases behind the round. The most straight-
forward method is to literally cork it. The plug, or sabot,
seals the barrel during firing and drops away once the projec-
tile leaves the muzzle. This method has been successfully
demonstrated but is not considered practical for use in modern
jet aircraft where the rejected sabot presents a serious haz-
ard if injested by the engine.

13

C. A SOLUTION

The ball-obturated tubular projectile offers a practical solution that is analogous to a common ball valve. The longitudinal hole is closed by a spherically seated ball while in the gun barrel and is opened by the spinning ball motion within the projectile after leaving the muzzle. The high spin rates developed in the barrel tend to throw the ball's mass away from the center of spin. As soon as the force of the expanding gases is released the ball, being in an unstable position, rapidly rotates about its mass centroidal axis and aligns its ports with the projectile tube.

This thesis is an extension of work started by Nunn and Bloomer [5,6] in which the equations governing the motion of the ball in response to the applied moments were developed. As stated therein a major goal of continuing research should be directed toward an understanding of the nature of the aerodynamic forces acting on the ball especially under partially-open ball conditions. It was for that purpose that this study was undertaken.

Initially it was hoped to develop an apparatus to measure lift, drag, and overturning moment acting on the ball. The supersonic wind-tunnel at the Naval Postgraduate School was designated to be used for this study.

The study was conducted with strut-mounted projectiles attached to a cantilever beam. Strain gages were used to determine beam displacement which allowed deduction of both

14

drag and overturning moment. A prototype 20-mm ball-obturated tubular projectile was modified so the ball could be rotated and pinned at predetermined positions during testing (Fig. 1). Tests were then run and coefficients of drag and overturning moment were calculated and plotted as functions of ball angle and Mach number.
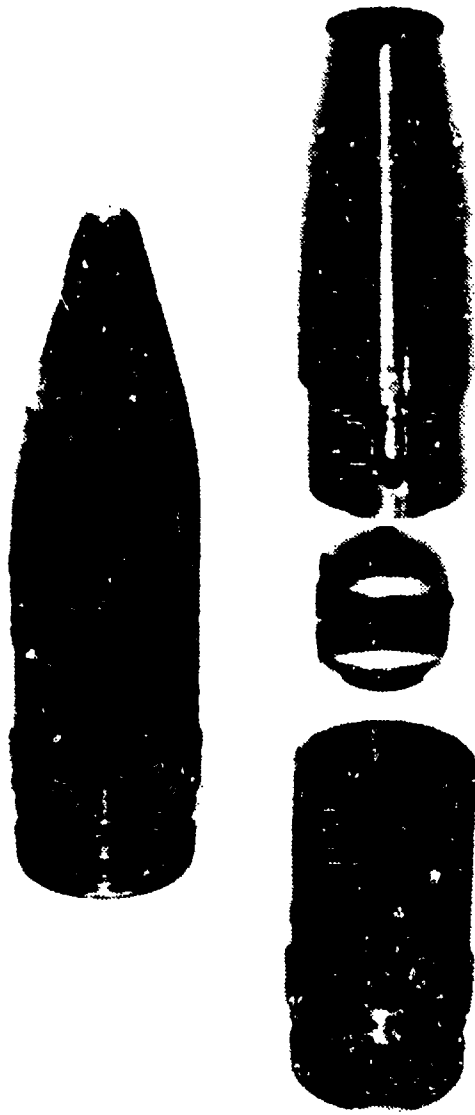
Figure 1. Conventional 20-mm and ball-obturated tubular projectiles modified for wind-tunnel testing.

16

II. EXPERIMENTAL APPARATUS

A. THE WIND-TUNNEL INSTRUMENTATION

The apparatus used for all testing is pictured in Figure 2 and depicted schematically in Figure 3. The wind-tunnel is of a fixed Mach number type with nominal test-section area of 0.1m square. Interchangeable nozzle blocks were used to allow tests at nominal Mach numbers of 1.94, 2.88, and 4.0.

A standard mercury and glass barometer was used to indicate ambient pressure after correction for temperature and gravitational variation. Another mercury manometer was connected to the tunnel wall about 10-cm upstream of the model in order to measure the test-section static pressure, P_w. The assumption was made that the static pressure at this point was representative of that in the test-section upstream of the projectile. The mercury column displayed magnitude of the tunnel test-section vacuum in inches of mercury below ambient pressure. The plenum pressure, P_o, was measured with a pressure transducer and the output signal recorded on a strip chart for the duration of each run. The strain gage outputs were recorded on an identical strip chart run at the same chart speed so that plenum pressure variations could be correlated with beam motion. In order to closely coordinate all three measurements, (strain gages, plenum pressure, and test-section vacuum), the

17
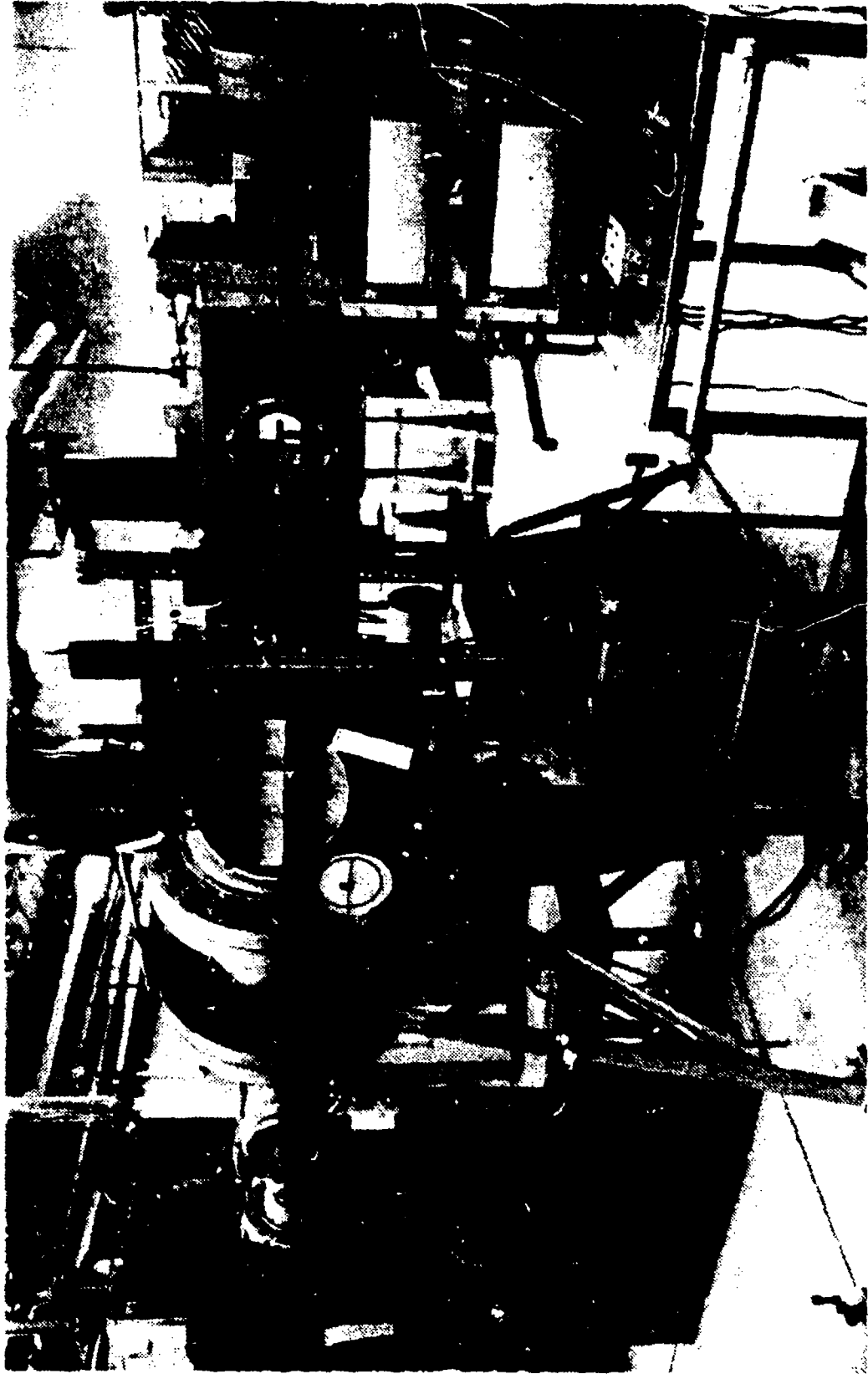
Figure 2. Experimental Apparatus

18
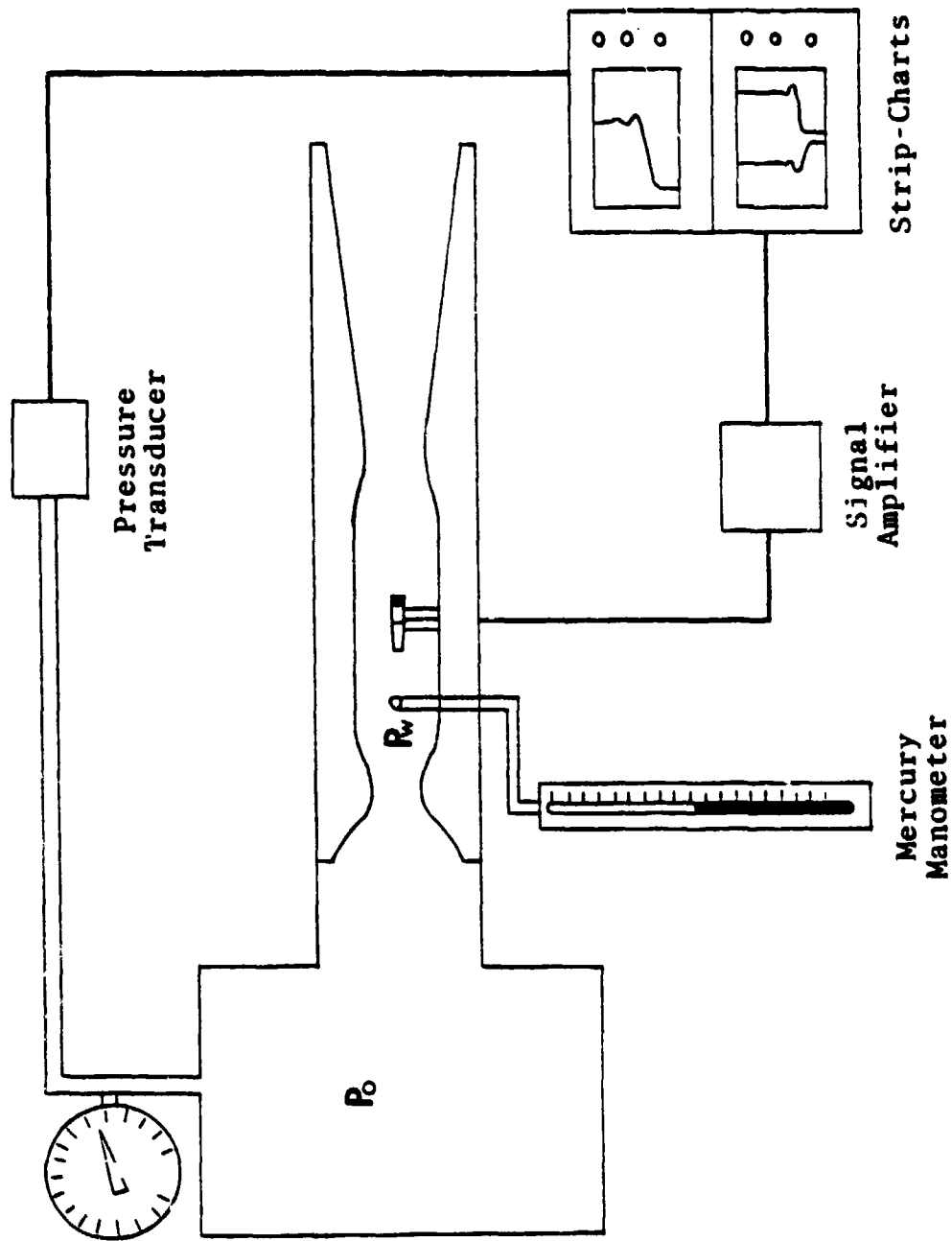
Figure 3. Schematic representation of experimental apparatus.

P_W column was read first and immediately the strip chart recording pens were lifted off the paper just long enough to leave a gap in the tracings to serve as an event marker.

A Schlieren optical system was used for flow visualization and a photograph was taken at each Mach number and ball setting. It was hoped the photographs would show correlation between measurements and observed flow phenomena.

B. THE BALANCE

Design of the balance constituted a major portion of the study. A variety of mechanical and electrical means for sensing pressure and force were considered. Design requirements for the balance were as follows:

1. Strength sufficient to handle drag forces estimated to be as high as 30N with adequate provision for transient peaks and design uncertainties.

2. Structural support for the projectile in the tunnel was to be obtained with a minimum of interference and flow obstruction.

3. An unobstructed view through the side ports was necessary to make the Schlieren photographs.

4. The nozzle block design allowed instrumentation to be inserted through the lower wall only; it was made of a workable phenolic while the upper block was solid steel.

5. The balance instrumentation had to be insensitive to environmental temperature, pressure and humidity changes.

6. The balance itself had to be sturdy enough to withstand possibly severe vibrations caused by turbulent shear and tunnel start-up transients.

7. Allowance was needed to provide for quick adjustments to the test projectile through the removable viewing ports.

8. The projectile support strut had to provide the smallest aerodynamic interference possible so its contribution to the total measured quantities was minimized.

9. The strain gage arrangement was to provide maximum sensitivity to aerodynamic forces while being of minimum size and relatively insensitive to spurious signals.

The initial design solution is shown in Figure 4 with a standard 20-mm projectile mounted on two struts. The design appeared to have a low-enough interference drag but was inadequate in three respects. First the baseplate, which acts as a fairing where the balance protrudes through the tunnel floor, was too thin and its bending was an unmeasured quantity that may have proved significant in the final analysis. Secondly the baseplate leading edge extended far enough forward that a shock wave formed there interfered with the mounted projectile. This shock is readily apparent in the Schlieren photograph, Figure 5, which shows the mount in the tunnel with a wedge body attached at Mach 2.9. Both of these shortcomings proved academic, as a

21

weakness in the silver-soldered joints at the strut/baseplate attachment resulted in the launch of a 20-mm projectile, with struts attached, down the tunnel at Mach 2.9.

The next design, shown in Figure 6 and in the design drawing, Figure 7, overcame these weaknesses with a thicker baseplate of minimum fore and aft dimension and a balance machined from a single piece of low carbon steel. The single strut was designed for minimum drag by maximizing the width dimension, (16.5 mm), and keeping it as thin as possible, (3.8 mm). The mount was also designed to maximize the distance, ℓ , from ball center to strut center. The longer this moment arm could be made the higher would be the moments experienced at the point of measurement. A further advantage of the new design was that the single wedge shaped strut lent itself to interference drag approximations by using standard compressible flow theory.

C. AERODYNAMIC FORCE AND MOMENT MEASUREMENT

The strain gages were mounted using standard techniques. Originally, each of four gages was wired to a separate recording channel and to an identical temperature compensating gage. The compensators were mounted as close as physically possible below the cantilever part of the balance. Temperature compensation proved inadequate with this gage configuration, however, because of the extreme sensitivity of the gages and the rapid temperature changes that occurred during tunnel start-up.

22

Figure 4. M56 projectile mounted in the wind-
tunnel on initial balance design.
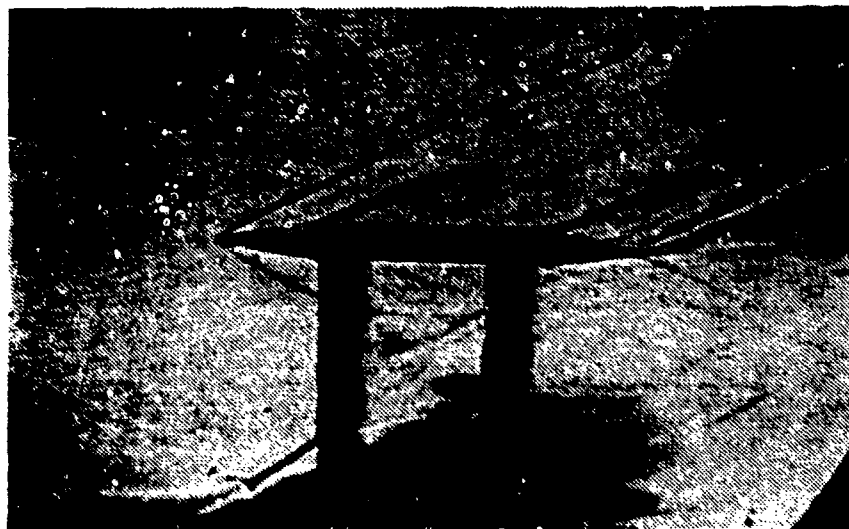
Figure 5. Schlieren photograph of initial balance
with double-wedge mounted at Mach 2.9.
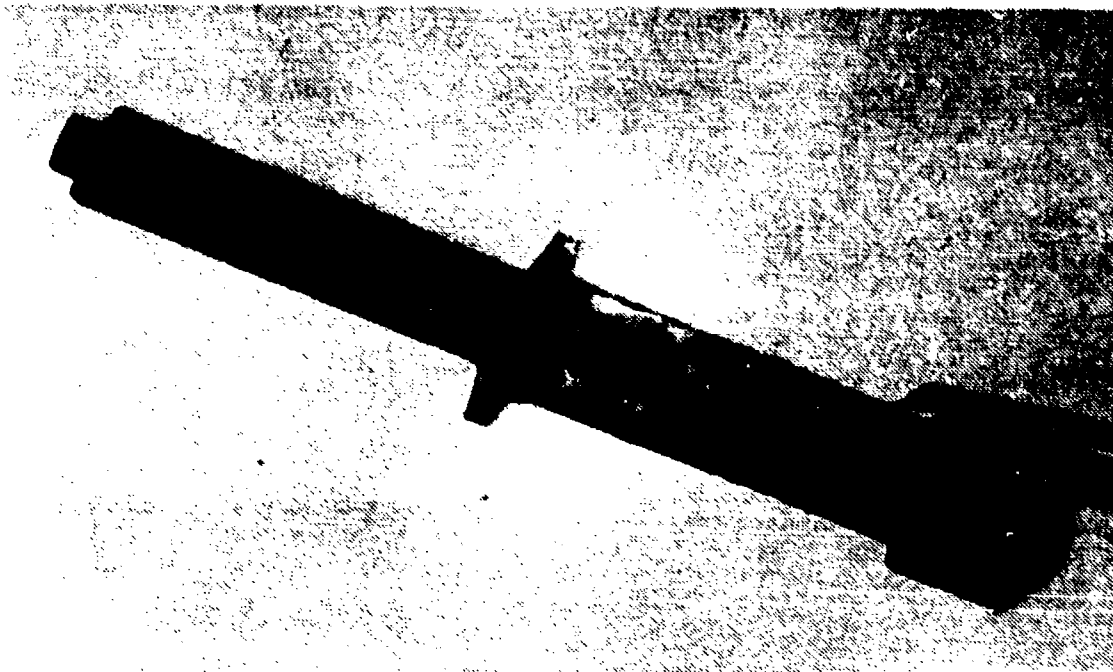
Figure 6.   Second balance design.
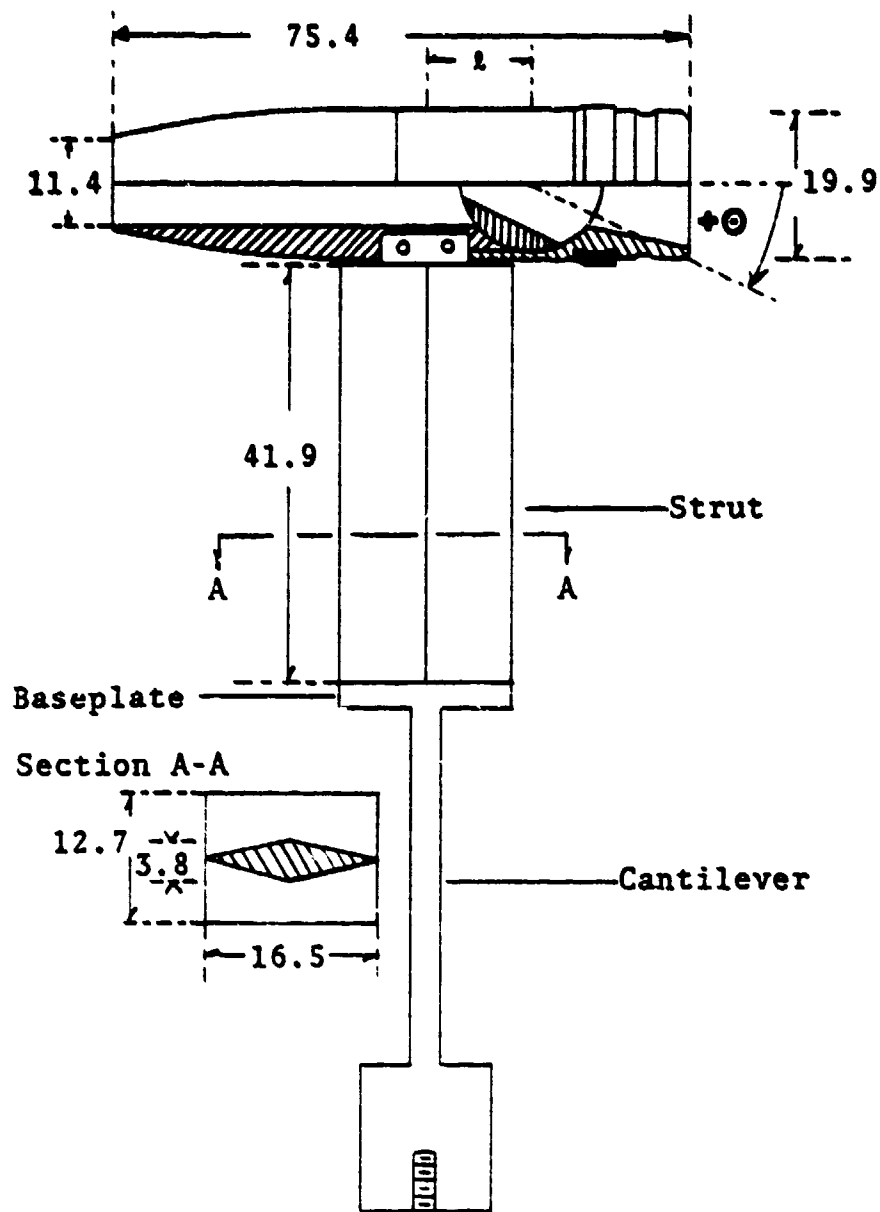
Figure 7.   Second balance design-sketch.
            All dimensions in millimeters.

The apparatus was very sensitive even to the temperature gradient established across the 2 cm-or-so distance between the recording gage and its temperature compensator. As a result, the recording channels would not hold a steady zero setting. The solution to this problem was to connect the two recording gages at the same height but on different sides of the cantilever to the same channel. The arrangement was wired so that one recording gage acted as the temperature compensator for the other. This worked out well because the temperature gradient between each pair of gages was only across the cantilever thickness - 3.0 mm. With four gages on four separate recording channels the theory for reducing the gage outputs to the three physical quantities, lift, drag, and overturning moment is as follows:

Y

M_∞

M

X

$\overline{V}_\ell$

$\overline{V}_u$

B | A

D | C
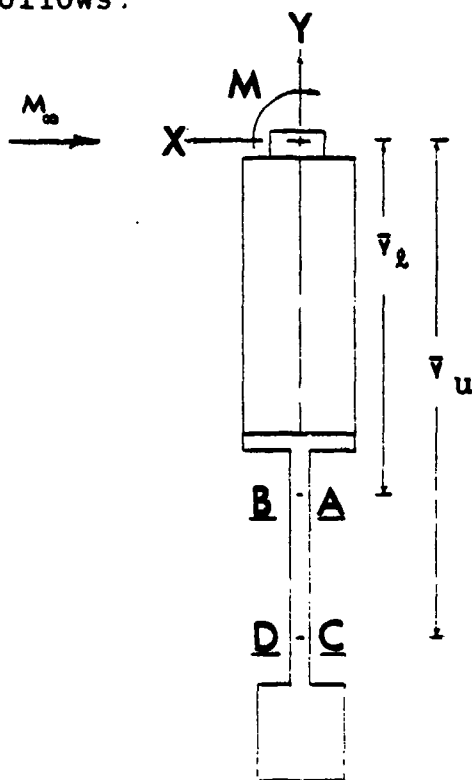
Let K_{jT} and K_{jM} be the proportionality constants between forces and moments and the gage signal outputs.

K_{jT} = gage j, tension

K_{jM} = gage j, bending

The outputs for gages A, B, C, and D are given as functions of force components in the X and Y direction and a moment, M, as follows:

26

$$A = K_{AT}\ Y + K_{AM}\ (y_A\ X - M)$$

$$B = K_{BT}\ Y - K_{BM}\ (y_B\ X - M)$$

$$C = K_{CT}\ Y + K_{CM}\ (y_C\ X - M)$$

$$D = K_{DT}\ Y - K_{DM}\ (y_D\ X - M)$$

where y_A, y_B, etc. are the distances between the moment center and the gage locations.

The four strain relationships may be combined to produce the three equations below:

$$A-B = Y(K_{AT}-K_{BT}) - M(K_{AM}+K_{BM}) + X(K_{AM}\ y_A+K_{BM}\ y_B) \tag{1}$$

$$C-D = Y(K_{CT}-K_{DT}) - M(K_{CM}+K_{DM}) + X(K_{CM}\ y_C+K_{DM}\ y_D) \tag{2}$$

$$A+B+C+D = Y(K_{AT} + K_{BT} + K_{CT} + K_{DT}) \tag{3}$$

$$+ M[(K_{BM} - K_{AM}) + (K_{DM} - K_{CM})]$$

$$- X[(y_B\ K_{BM} - y_A\ K_{AM}) + (y_D\ K_{DM} - y_C\ K_{CM})]$$

If all gages are assumed identical, then,

$$K_{AT} = K_{BT} = K_{CT} = K_{DT}$$

and

$$K_{AM} = K_{BM} = K_{CM} = K_{DM}$$

so that equations (1), (2), and (3) are simplified to:

$$A-B = K(\overline{y}_u\ X - M) \tag{3}$$

$$C-D = K(\overline{y}_\lambda\ X - M) \tag{4}$$

27

$$\Sigma = A+B+C+D = K_1 Y - \frac{K}{2} X[(y_B - y_A) + (y_D - y_C)] \qquad (5)$$

where $\quad K = K_{AM} + K_{BM} = 2K_{AM}$

$$K_1 = K_{AT} + K_{BT} + K_{CT} + K_{DT}$$

and $\quad \bar{y}_u = \dfrac{y_A + y_B}{2} \qquad\qquad \bar{y}_\ell = \dfrac{y_C + y_D}{2}$

Finally these relationships may be combined and solved for the forces and moment as follows:

<u>Drag</u> $\quad X = \dfrac{(C-D) - (A-B)}{K(\bar{y}_\ell - \bar{y}_u)} \qquad\qquad (6)$

<u>Lift</u> $\quad Y = \dfrac{1}{K_1} [\Sigma + \dfrac{KX}{2} [(y_B - y_A) + (y_D - y_C)]] \qquad (7)$

<u>Moment</u> $\quad M = \dfrac{\bar{y}_u (C-D) - \bar{y}_\ell (A-B)}{K(\bar{y}_\ell - \bar{y}_u)} \qquad\qquad (8)$

When the shift was made to two recording channels vice four, lift could no longer be measured because it was no longer possible to obtain the Σ value required above.

Although lift was a desired quantity it could have not have been measured with much accuracy using the chosen balance design. A pure lift measurement would require determining how much the steel cantilever beam was stretched. The lift force due to rotation of the ball within the projectile, and esti-mated to be less than .2N, would not produce an output signal

28

high enough to separate it from spurious noise signals in the
balance instrumentation. (At that lift force the cantilever
would experience a strain of 0.26 microstrains.) In addition
to improved temperature compensation, a major advantage to
using two gages on each recording channel was that the ampli-
tude of the output, now equal to the difference in the gage
outputs, was doubled so that a much higher signal-to-noise
ratio was obtained. Also the arithmetic difference of gage
pair outputs was now performed by the circuitry and thus
another possible source of error was eliminated.

D. INTERFERENCE DETERMINATION

The final major problem encountered in the testing proce-
dure was that of determining what part of the total measured
drag and moment was caused by the projectile alone. Deviations
of the total measured quantities from those due to the projec-
tile alone were assumed to result from balance, tunnel, and
projectile interactions and will be referred to as tare
quantities. The interactions included form and frictional
drag on exposed balance parts, flows through small gaps between
baseplate and tunnel floor, shock waves formed on the baseplate
leading edge and unknown pressure gradients across the test
section.

Several methods were considered to estimate these "tare"
quantities. The first method involved attaching a test body
to the strut that has theoretically well-established drag

properties such as the double-ended wedge shown in Figure 5. Unfortunately the basic theory is for an infinite span wedge while the test section could, of course, only accommodate a somewhat shorter one. The maximum aspect ratio possible was about eight and then the tips of that wedge would be intruding into the less uniform flow at the boundaries of the test section side wall. Further, there would be considerable deviation from theory due to effects such as tip vortices and cross-flow drag if the angle-of-attack was any value but zero. A double-ended cone might have reduced the number of unknown flow effects but, as with the wedge, there would still be the question of the flow interaction at the test-body/strut attachment. It was finally decided to use a standard M56 20-mm projectile for which the drag had been measured in actual firing tests [7]. The overturning moment, M, was assumed to be zero for this standard. It was realized, however, that probable pressure differences existed between top and bottom of the projectile caused by the strut attachment. This pressure imbalance would result in a lift force and possibly some overturning moment. The problem of the resulting nonzero moment is addressed in the experimental results section.

Before each new series of runs the projectiles were checked for zero angle of attack with a surveyor's transit while mounted in the tunnel. It should also be noted that, inherent in the balance design, some angle of attack is created whenever a drag

30

force is experienced by the projectile or strut. This occurs because the anchored end of the cantilever causes the strut tip to swing through some arc, however small, whenever the projectile is displaced from the no-load position. Standard beam bending formulas were used along with an estimated force loading to estimate the change in angle of attack. The small fraction of a degree obtained was considered negligible for these "first-cut" tests.

The calibration of the balance was accomplished using the test rigs shown in Figure 8 and Figure 9. In the first case a pure drag-type force was applied, and in the second a pure moment. The results were reduced to provide the constant of proportionality, K, required by the linear relationships for drag and moment. A sample calibration is included in Appendix B.

E. THE TUBULAR PROJECTILE WIND-TUNNEL MODEL

The tubular projectile was modified so that the ball was restricted to rotation about its pitch axis only. It could be pinned in nine different rotation angles, Θ , by use of a set screw and dimples machined into the ball. The finished product is shown in Figure 1 along with the standard 20-mm projectile. Figure 7 includes a cross sectional drawing of the modification. Notice the direction of positive Θ . A tang at the top of the strut was inserted into a grove in the projectile and the two were secured with a pair of shear pins. In spite of close machining tolerances some sloppiness of fit

31
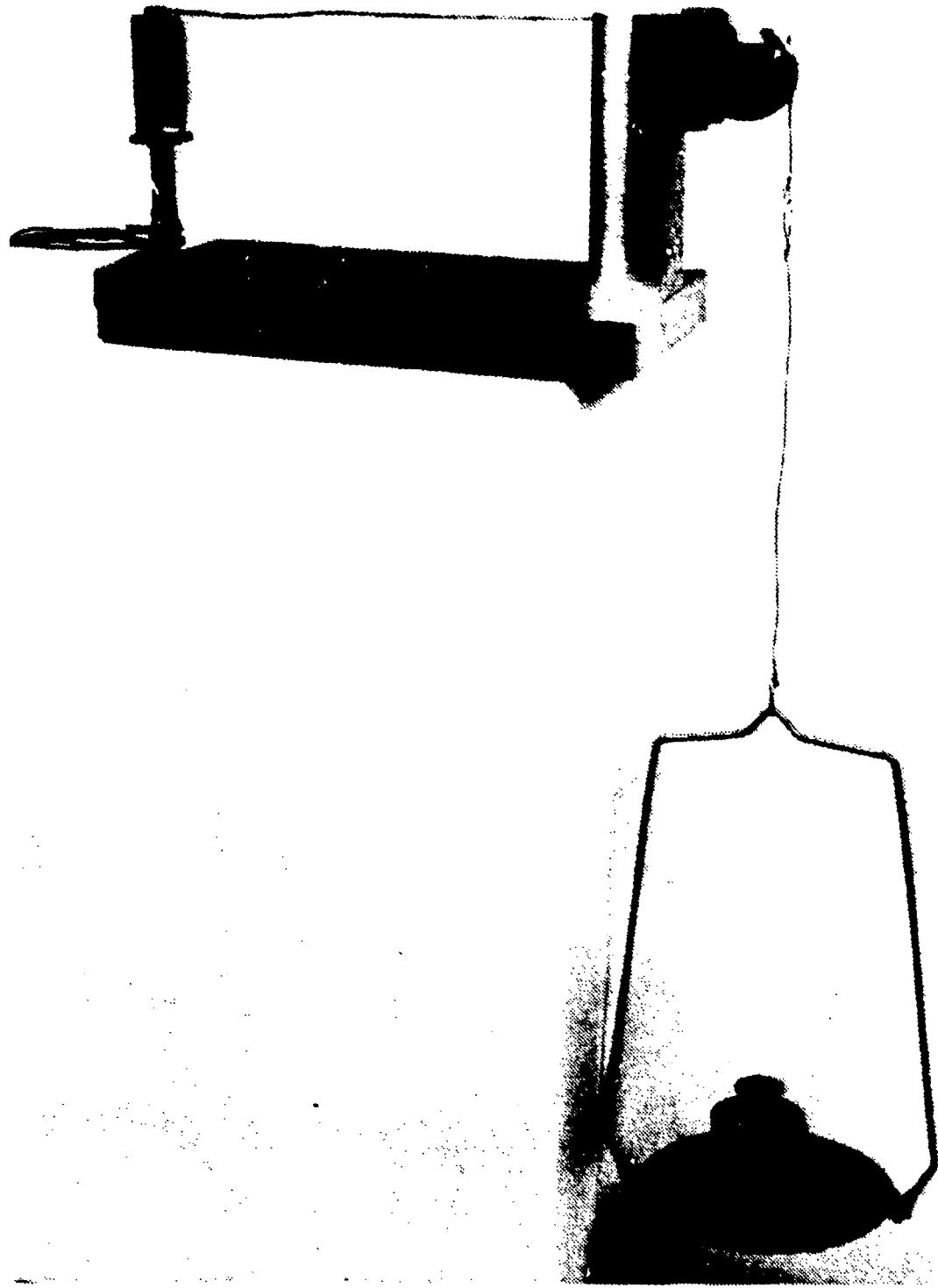
Figure 8. Drag calibration apparatus.
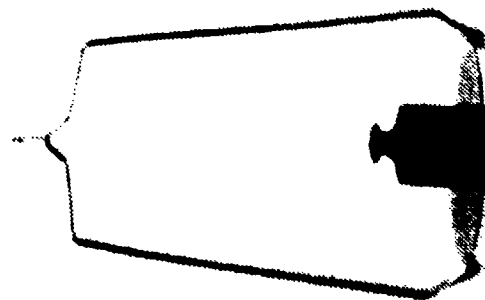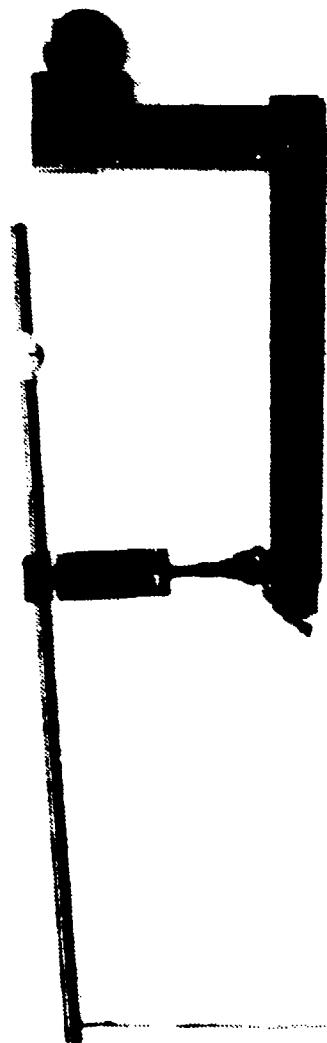
Figure 9. Moment calibration apparatus.

33

was present as the projectile could be rocked slightly about its pitch axis while on the strut. This unwanted motion was taken-up by building a seat for the projectile on top of the strut with solder and epoxy. The stiffness of the mount improved with test experience so that the Mach 1.94 data is more free from this effect than the data of the Mach 2.88 series, and the Mach 4.0 data should be the best of all.

III.   EXPERIMENTAL RESULTS

A.   PROJECTILE DRAG

1.   Corrections to Total Drag (C_{D_T})

a.   Reference Coefficient Correction $(C_{D_{TA}})$

The measured total drag coefficient was corrected with a reference coefficient for the standard M56 20-mm as follows:

$$C_D = C_{D_T} - C_{D_{TA}}$$

where

$$C_{D_{TA}} = C_{D_{TS}} - C_{D_{PR}}$$

and

C_D = projectile drag coefficient

C_{D_T} = total measured drag coefficient

$C_{D_{TA}}$ = interference drag coefficient, (Table I)

$C_{D_{TS}}$ = total measured drag for an M56 projectile

$C_{D_{PR}}$ = reference drag coefficient for an M56 projectile

b.   Estimated Values of Drag Correction Coefficients

The interference drag coefficient was checked by comparison with a theoretically calculated tare drag based on elementary compressible flow methods for the strut, (a double

35

wedge in cross-section). This theoretical estimate, $C_{D_{TH}}$, is compared with the experimentally determined tare drags in Table I.

Table I. Drag Coefficient Correction Comparison

M_∞	$C_{D_{TS}}$	$C_{D_{PR}}$*	$C_{D_{TA}}$	$C_{D_{TH}}$
1.94	.820	.465	.355	.288
2.88	.648	.388	.260	.183
4.0	.476	.316	.160	.136

*The reference drag coefficient for M = 4.0 was obtained through private communication with the Naval Weapons Center, China Lake, CA, Code 3247. Values at other Mach numbers are those reported in [7].

Notice that the theoretical tare drags are less than those derived from experimentation. This is as expected because the theory is for a double-wedge of infinite span while the flow across the strut is complicated by many factors such as interference from both the projectile and tunnel floor.

2. Presentation of Results

Figures 10, 11, 12, and 13 show C_D as a function of Θ . The ball is full open at Θ = 0 and full closed for values of Θ greater than 75 degrees. The uncertainty band calculations were performed as recommended by Ref. [8], and were based on results for the ball angle giving the most-scattered data for each Mach number. Table II gives numerical values for the maximum fractional uncertainty associated with the major experimental parameters.
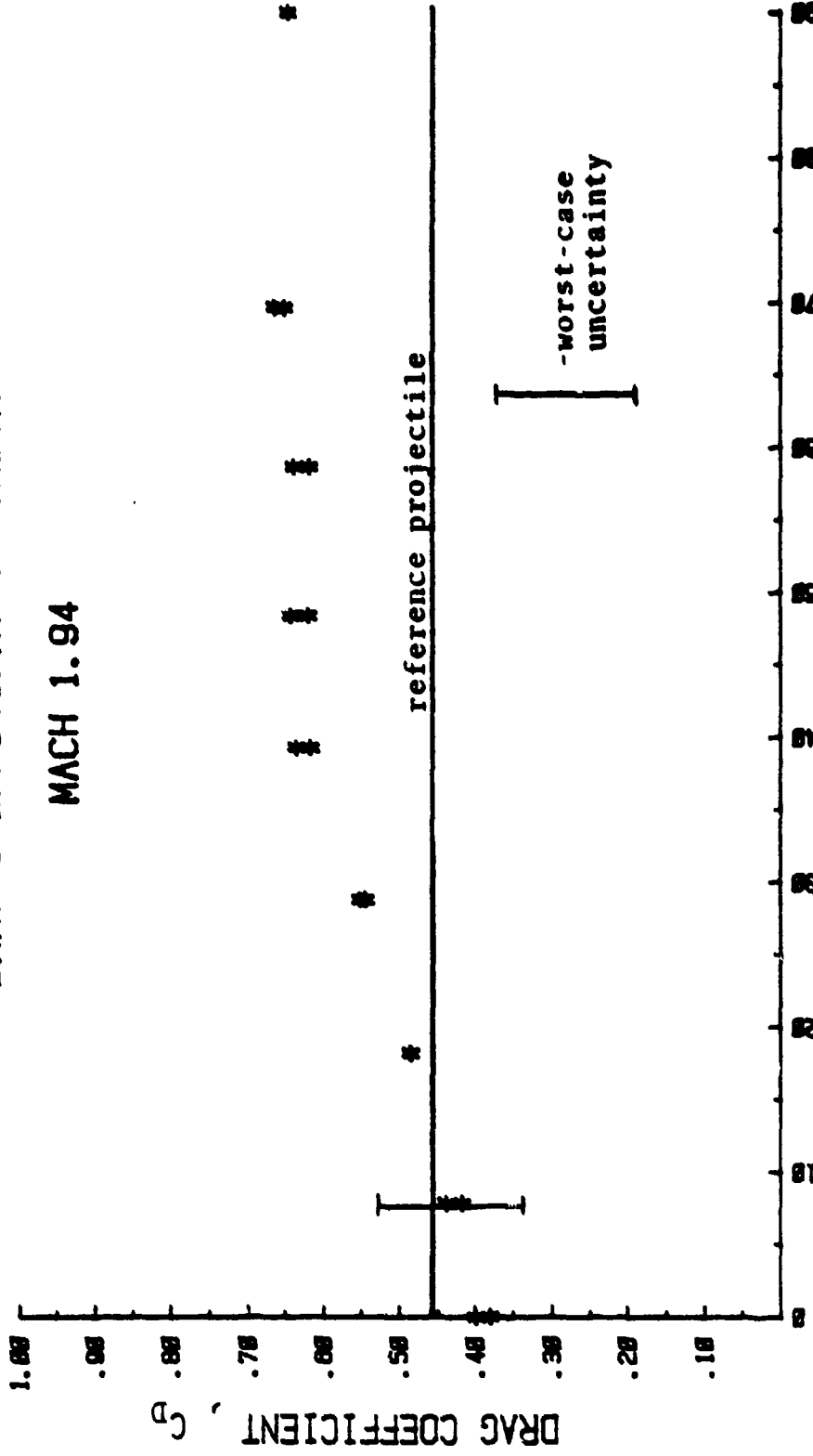
Figure 10. Drag Coefficient vs. Ball Angle. $M_\infty = 1.94$.
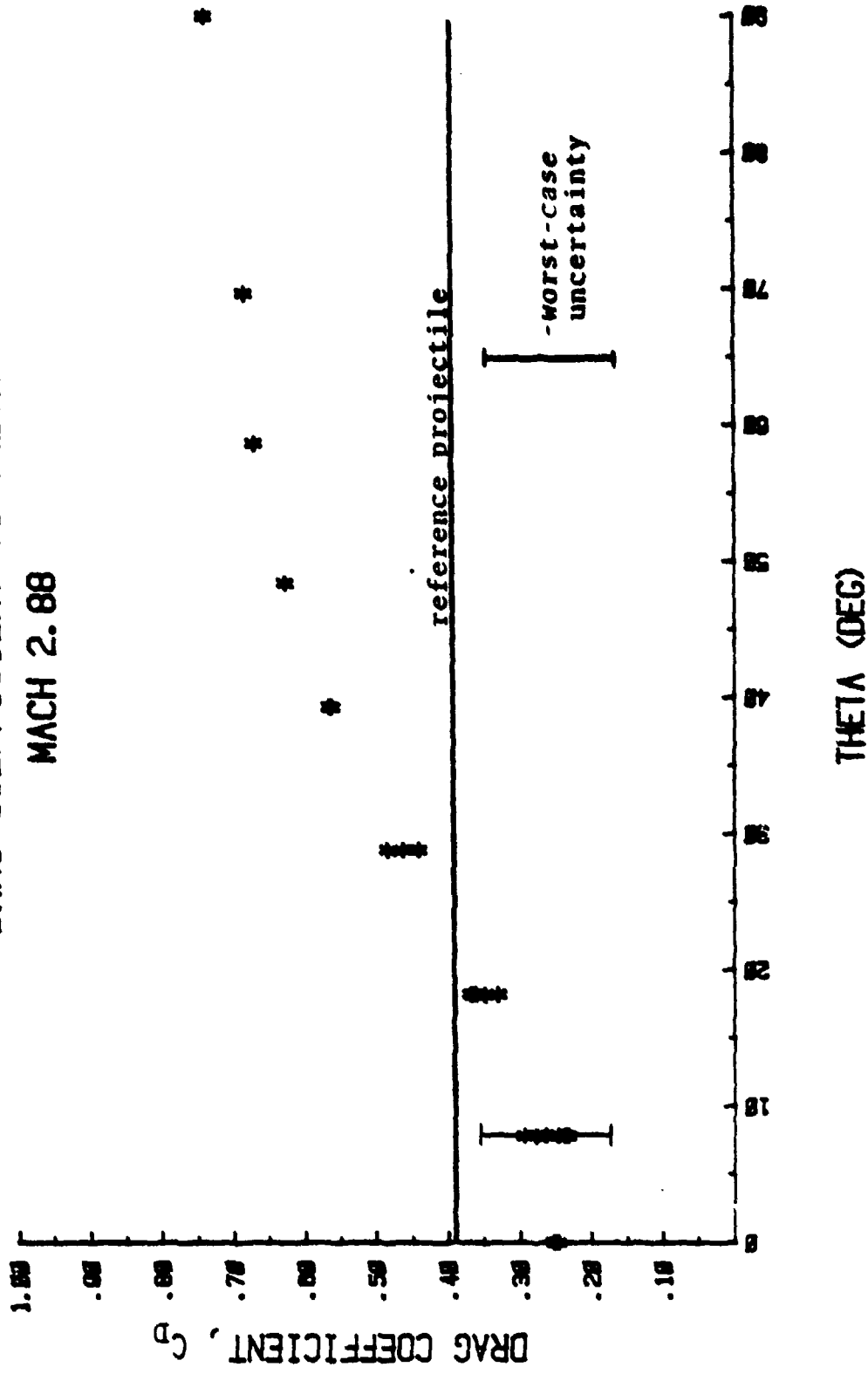
Figure 11. Drag Coefficient vs. Ball Angle. $M_\infty = 2.88$.
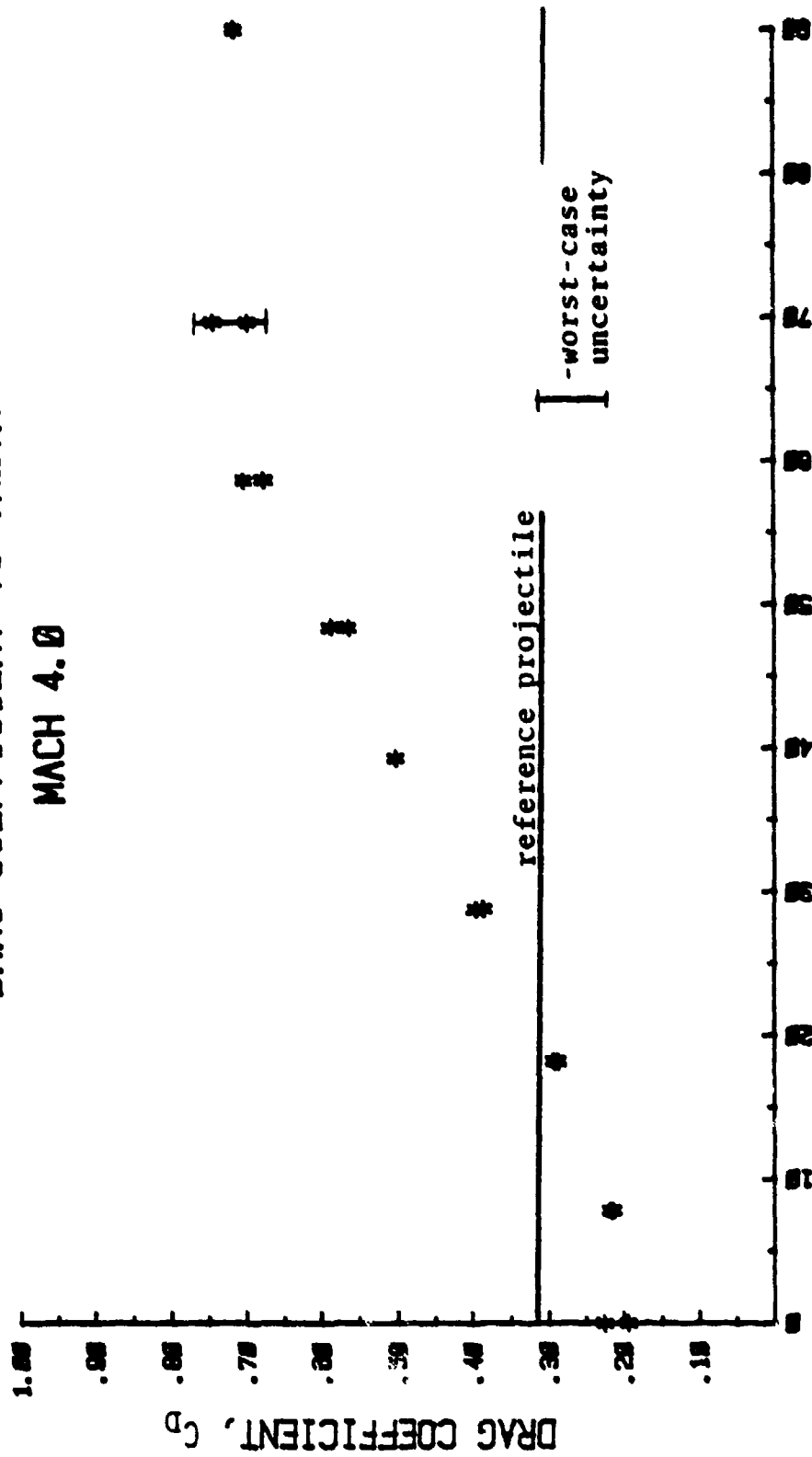
Figure 12. Drag Coefficient *vs.* Ball Angle. $M_\infty = 4.0$.
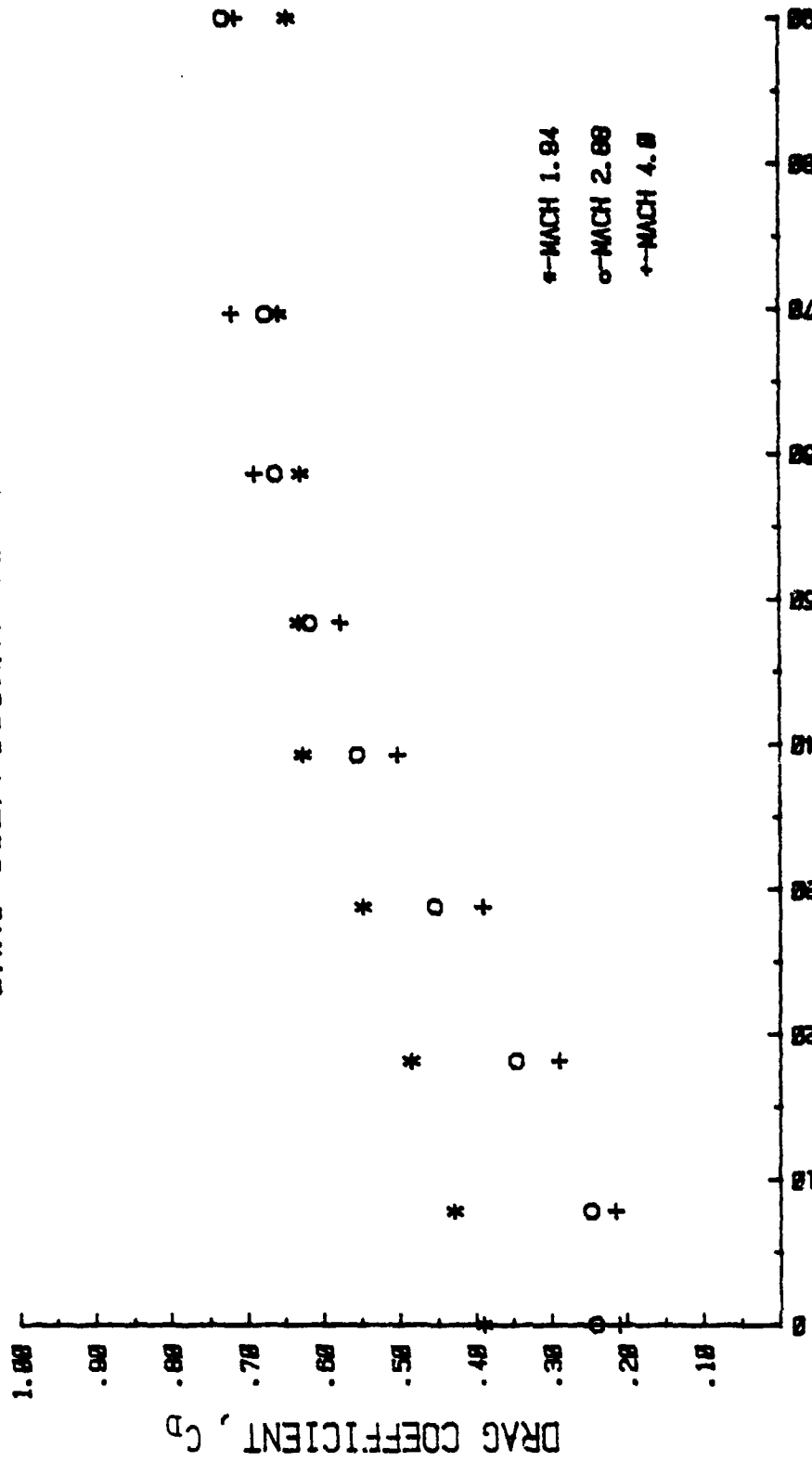
Figure 13. Mean Drag Coefficients vs. Ball Angle, Combined.

40

Table II. Drag Coefficient Uncertainty (worst case)

M_∞	$\dfrac{\Delta P_W}{P_W}$	$\dfrac{\Delta M_\infty}{M_\infty}$	$\dfrac{\Delta D}{D}$	$\dfrac{\Delta C_D}{C_D}$
1.94	.064	.022	.099	.126
2.88	.062	.014	.155	.169
4.0	.031	3.55 E-5	.04	.05

a. Observations

These data indicate the following trends and effects:

(1) The drag coefficient at ball angles up to 50 degrees decreases with increasing Mach number. At higher ball angles, the trend with Mach number may be obscured by experimental uncertainty.

(2) The drag approaches a constant value as Θ approaches 90 degrees (the closed position) at any given Mach number.

(3) The full-open ball position does not have a drag coefficient that is appreciably lower than that of the reference projectile at Mach 1.94.

(4) The drag coefficient with the ball fully open is appreciably reduced at Mach 2.88 and 4.0.

(5) As illustrated by the combined plot of mean drag coefficient values, Figure 13, the drag coefficient for the closed-ball position is lower at Mach 1.94 than at the

higher Mach numbers. With the ball open, though, the Mach
1.94 drag coefficient exceeds the higher Mach number values.
Discussion of these results is continued in Section IV.

B. PROJECTILE OVERTURNING MOMENT

1. <u>Corrections to Total Moment</u> (C_{M_T})

a. Standard Projectile Correction

The total measured moment coefficient was corrected
with a tare value obtained from tests of the standard M56 20-mm
projectile. The mean of the measured values for $C_{M_{TA}}$ was used
for each Mach number, and the tubular projectile overturning
moments were estimated as follows:

$$C_M = C_{M_T} - C_{M_{TA}}$$

where

C_M - Projectile overturning moment coefficient.

C_{M_T} - Total measured overturning moment coefficient.

$C_{M_{TA}}$ - Interference moment coefficient (Table III).

Table III. Moment Coefficient Correction

Mach	$C_{M_{TA}}$
1.94	-.2308
2.88	.0802
4.0	-.0549

The above corrections assume that the standard projectile has zero overturning moment. As the results show, Appendix A, this was not the case. It is probable that any small angle-of-attack, α , resulted in just such a moment. The angle-of-attack was set at zero in the shop and confirmed in place. Even so, a small deviation from zero could go undetected. In any case, as a result of projectile drag, a small angle-of-attack was developed as the strut was displaced from a no-load position.

2. Presentation of Results

Figures 14, 16, and 18 show C_M as a function of θ for the three test Mach numbers. The worst-case values for the uncertainty bands appear in Table IV. (The values for $\Delta M_\infty / M_\infty$ and $\Delta P_w / P_w$ are identical to those used in the drag calculations and are not repeated here.)

Table IV.   Moment Coefficient Uncertainty (worst case)

M_∞	$\dfrac{\Delta M}{M}$	$\dfrac{\Delta C_M}{C_M}$
1.94	1.21	1.21
2.88	1.02	1.02
4.0	2.24	2.24

Each of the moment coefficient plots is followed by a series of Schlieren photographs for flow visualization comparisons as the ball is closed down. The bottom right picture of each series is the standard 20-mm projectile.

a. Observations

In spite of the prohibitively large uncertainties in these measurements, a few trends are worth noting:

(1) The tare moments for Mach 1.94 and 4.0 are both negative, (pitch down).

(2) The moment coefficients become positive as the ball is closed down.

(3) Both the Mach 2.88 and 4.0 plots show C_M to be negative at the full open ball position yet it is positive at Mach 1.94.

(4) The moment coefficient appears to reach a maximum value at about the point of maximum bow-shock detachment, (see Schlieren series).

(5) All curves demonstrate consistent behavior in that they rise rapidly as θ is increased. Then all reach a maximum and dip down again before recovering to somewhat higher values.

(6) The uncertainty bands are exceedingly large and all are dominated by the $\Delta M/M$ term.

MOMENT COEFFICIENT vs THETA

MACH 1.94

MOMENT COEFFICIENT, C_M

THETA (DEG)

worst-case uncertainty

tare moment
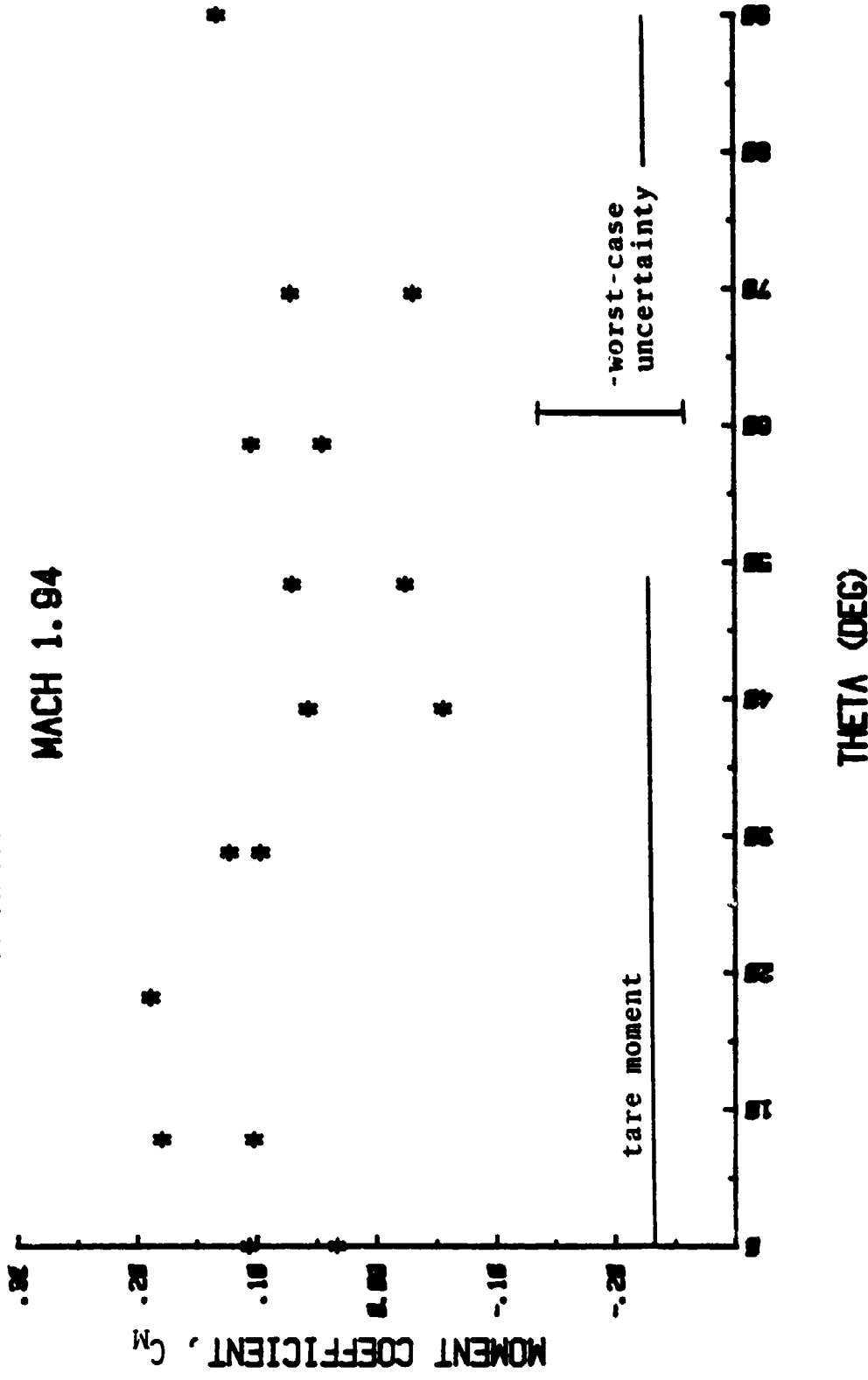
Figure 14. Moment Coefficient vs. Ball Angle. $M_\infty = 1.94$.
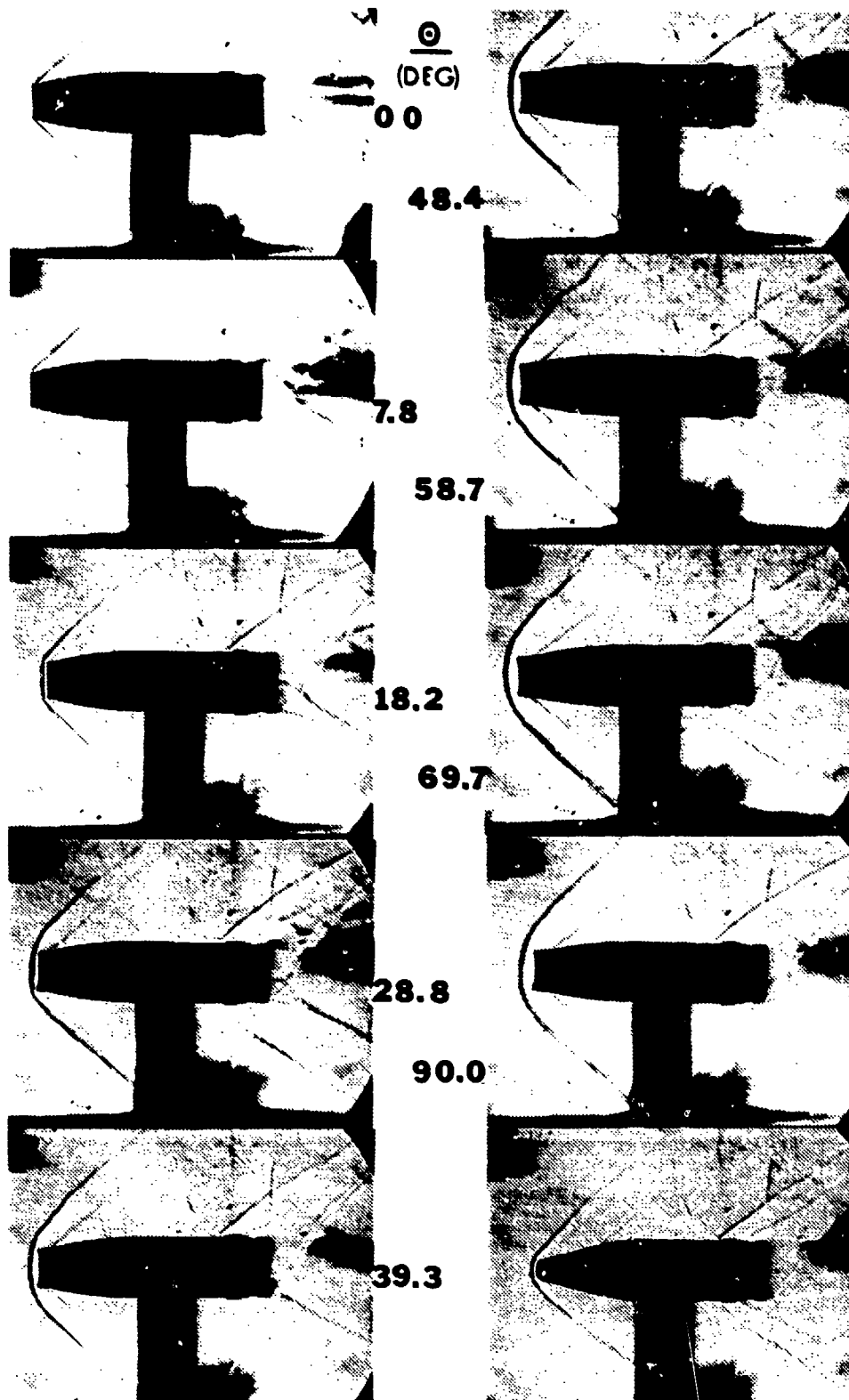
Figure 15. Schlieren series - Mach 1.94.

MOMENT COEFFICIENT vs THETA
MACH 2.88

tare moment

-worst-case uncertainty

MOMENT COEFFICIENT, c_M
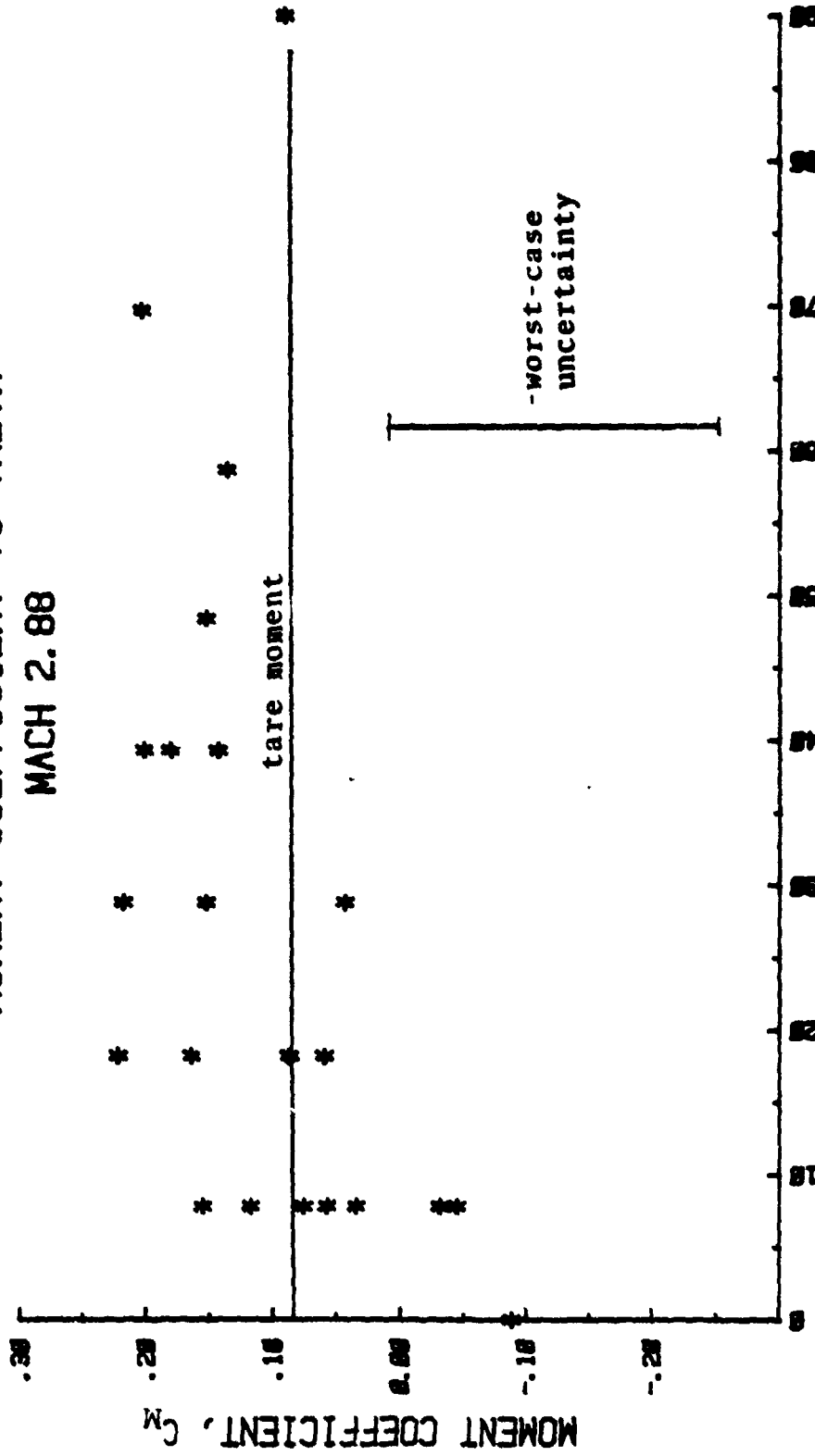
THETA (DEG)

Figure 16. Moment Coefficient vs. Ball Angle. $M_\infty = 2.88$.

47
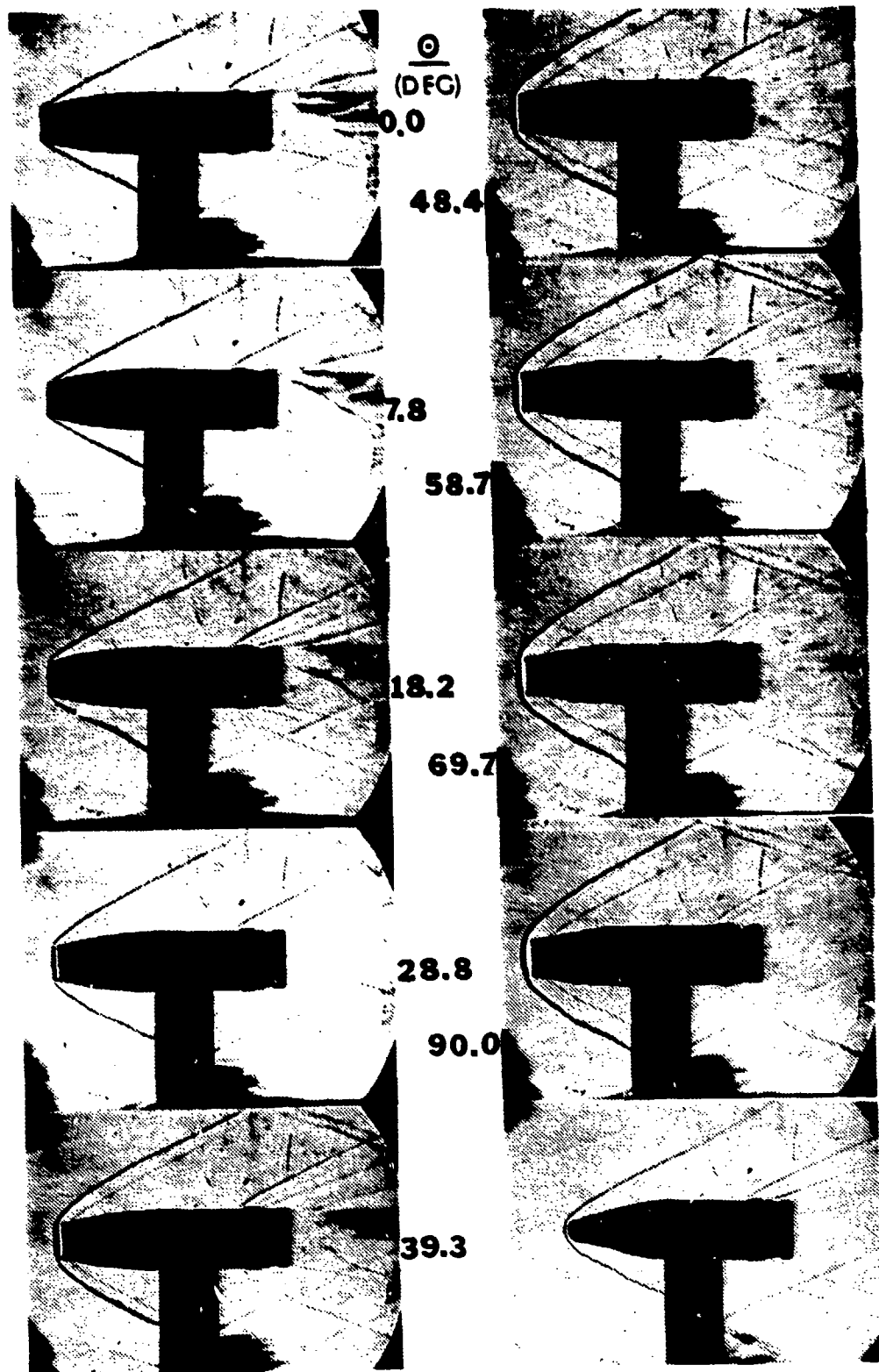
Figure 17. Schlieren series - Mach 2.88.

48

Figure 18. Moment Coefficient vs. Ball Angle. $M_\infty = 4.0$.
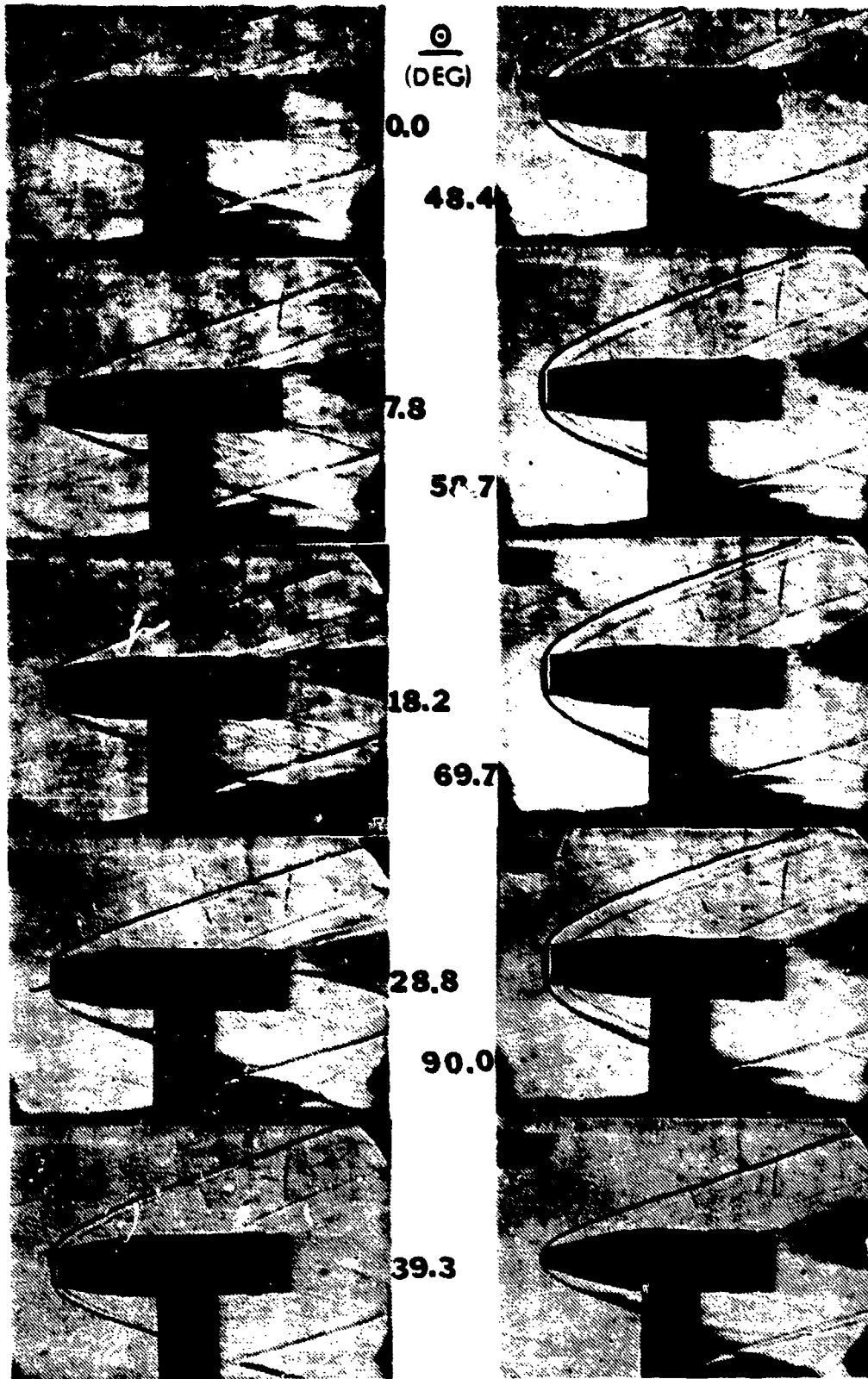
Figure 19. Schlieren series - Mach 4.0.

IV.   DISCUSSION OF RESULTS AND RECOMMENDATIONS

A.   DRAG COEFFICIENT

1. As the ball closes, the drag coefficient shows a tendency to rise sooner at the lower Mach numbers. Interestingly, the point where the curves change from a distinct positive slope to an asymptotic behavior occurs somewhat after initial bow shock detachment. This is well after the point where supersonic flow is no longer expected within the projectile.

2. The bow shocks appear at lesser ball angles at the lower Mach numbers, as expected.

3. A more precise study should incorporate a balance that eliminates the induced angle-of-attack problem. Even though it may be small under the given loads, its effect is still present and makes some contribution to the measured drag.

4. Figure 13 shows that the Mach 1.94 curve crosses the other two at about $\theta = 50$ degrees. Thereafter it continues to be the lowest in drag coefficient of the three. This may be explained by the fact that with the ball fully closed the projectile behaves more like a blunt object. Without the advantages of a streamlined projectile the drag increases as the pressure rise across the bow shock increases with Mach number. Therefore the blunt body drag becomes the predominant part of the total drag for the higher ball angles.

5. The same reasoning may be used to explain why a greater drag reduction is indicated for the full open ball position at Mach 4.0 than at the lower Mach numbers. The conventional M56 round has a somewhat blunt shaped nosecone. In a small region near the apex of that cone the pressure distribution may be approximated by blunt-body behavior; that is, the ratio of pressures across the shock is about equal to the ratio across a normal shock. The ratio of pressures across a normal shock is 4 times higher at Mach 4 than at Mach 2. Therefore when this region is removed, as it is in a tubular projectile, the drag reduction will be greater at the higher Mach numbers.

B. MOMENT COEFFICIENT

1. The negative tare moments for Mach 1.94 and 4.0 are probably due to inadequate correction of the data for the drag of the strut. Strut drag can be thought of as a force acting at some point below the projectile at some unknown moment arm. Any tipping up of the projectile would be expected to give a positive moment. The drag of the strut itself must have created a negative moment sufficient to overcome the expected positive moment encountered by the standard 20-mm round as it was pitched-up.

2. The fact that the moment coefficients for the full-open ball become increasingly negative for higher Mach numbers is puzzling and indicates the need for a better determination of tare moment.

3. All the moment data are suspect and the width of the uncertainty band leaves much room for conjecture. One possible source of error was the less-than-perfect projectile/strut attachment. It was modified with successive tests but, as the uncertainty bands show, no improvement was observed. In fact $\Delta C_M/C_M$ is at its worst value at Mach 4.0, the last series run.

The high value produced by the uncertainty analysis for the overturning moment is dominated by one term, $\Delta M/M$. This term is given by

$$\frac{\Delta M}{M} = [(\frac{\overline{y}_u}{M_c} \Delta (C\text{-}D))^2 + (\frac{\overline{y}_\ell}{M_c} \Delta (A\text{-}B))^2]^{1/2}$$

where

$$c = K(\overline{y}_\ell - \overline{y}_u)$$

Moment is given by equation (8) as:

$$M = \frac{\overline{y}_u (C\text{-}D) - \overline{y}_\ell (A\text{-}B)}{c}$$

The numerator, a difference of products, is extremely small because both terms are   nearly identical in magnitude. An example will help to clarify this point. At Mach 1.94 and Θ = 7.83 the following values were obtained:

$$C\text{-}D = 18.5$$
$$A\text{-}B = 12.8$$

53

This gives the following numerator for equation (8):

$$5.74 \ (18.5) - 8.23 \ (12.8) = .846$$

the value for $\bar{y}_u$ and $\bar{y}_\ell$ were obtained from the balance calibration, (see Appendix B). The resulting moment is then:

$$M = \frac{.846}{-.345} = -2.45 \ N \ cm$$

For this Mach number and ball angle the scatter of the data spans a moment range of approximately $\pm 3.6 \ N \ cm$. Under such circumstance the present balance design to ineffective as a moment measuring device.

The magnitude of the $\Delta C_M/C_M$ term can best be reduced by greatly increasing the distance $\bar{y}_\ell - \bar{y}_u$ or, more practically, by increasing M. Because M is a function of the distance of ball-center to strut-center, (the distance ℓ in Fig. 7), it is clear that increased accuracy cannot be readily obtained with the current design. This moment-arm is already about as large as the projectile's physical dimensions allow.

4. The moment coefficients were expected to be zero with the ball full open and full closed. The fact that they both vary considerably from expected values is further indication that the interference of the test-rig must be re-evaluated. It was previously noted that the curves follow a general behavior of starting at low values, peaking, and again dipping down. Because the $\Theta = 0$ position is lower than expected while

54

the $\Theta \approx 90$ is higher than expected (see Fig. 18, for example)
it is as if the entire expected curve has been rotated. Intui-
tively it seems that this general increase in C_M with Θ may be
an effect of the pitch-up of the projectile caused by the
higher drag at higher ball angles.

   Induced angle-of-attack calculations were made using
both maximum and minimum drag values at all three Mach numbers.
The calculations employed measured drag, compressible flow
estimates for strut drag, and standard beam bending estimates.
The results appear below:

Table V. Angle-of-Attack Estimates

Mach No. M_∞	Ball Angle Θ [deg.]	Total Drag D [N]	Strut Drag D_S [N]	Angle-of-Attack α [deg.]
1.94	69.67	22	6.4	.3
1.94	0	16	6.3	.19
2.88	90	20	3.7	.27
2.88	0	10	3.6	.15
4.0	69.67	20.9	3.1	.27
4.0	0	8.5	3.0	.13

   These results confirm estimates that the angle-of-attack
would be small although it appears they are not insignificant
in their effects upon overturning moments.

C. BALANCE DESIGN REQUIREMENTS RESTATED

A new balance to more accurately measure the overturning moment would incorporate the following:

1. The distance from ball-center to measurement point should be increased greatly to provide a greater moment-arm.

2. A means should be made for zeroing the angle-of-attack with the ball full open while operating the tunnel.

3. The ball should be remotely positionable so its angle can be controlled while "in-flight" in the tunnel. This might be accomplished with a speedometer-type cable passing through the support struts.

4. The support struts must be arranged symmetrically about the projectile so that the flow interference at each attachment point is cancelled by another.

Such a design might appear as shown in Figure 20.
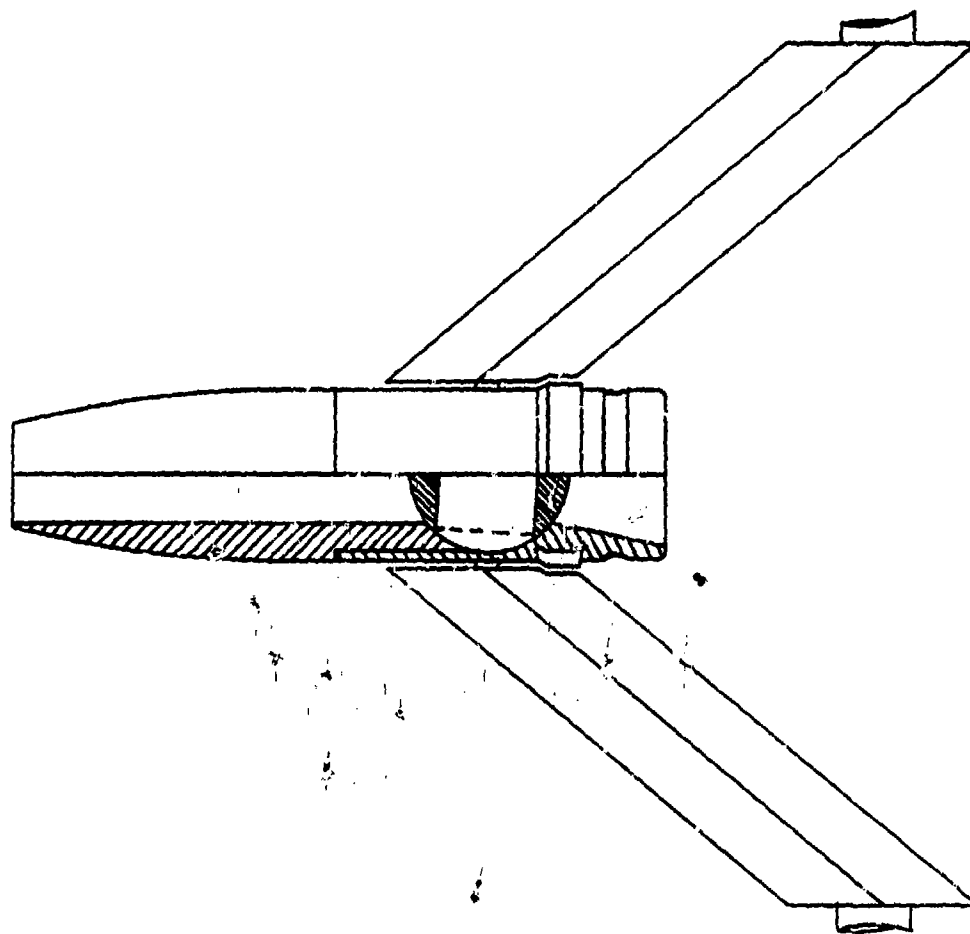
Figure 20.   Proposed balance design.

57

V. CONCLUSION

The results of this study show that the drag coefficients for the ball-obturated tubular projectile tested may or may not be lower than the equivalent conventional round depending on the Mach number and the position of the ball. Further, the drag coefficient increases at a given Mach number as the ball is closed down and approaches a constant value after complete bow-shock detachment.

The balance designed for this study may be used for reasonable approximations of drag but it is inadequate for overturning moment determination. A new balance design is required which incorporates a moment-arm long enough to amplify the small lift forces and moments developed by the ball.

APPENDIX A

Table A1 Reduced Data, Mach 1.94.

Θ (deg)	P_O (KP$_a$) abs	P_w (KP$_a$) abs	M_∞	$|X|$ (N)	C_{D_T}	M (N cm)	C_{M_T}
0	188.0	26.6	1.94	15.957	.7357	-5.385	-.1247
0	186.9	26.4	1.94	16.247	.7540	-8.498	-.1981
7.83	186.0	26.2	1.94	16.537	.7716	-2.197	-.0515
7.83	186.9	26.4	1.94	17.117	.7941	-5.526	-.1288
18.21	185.9	26.2	1.94	17.988	.8394	-1.831	-.0429
18.21	185.9	26.3	1.94	17.988	.8388	-1.831	-.0429
28.81	187.6	26.4	1.94	19.438	.8989	-5.809	-.1349
28.81	191.3	27.2	1.93	20.019	.9058	-4.794	-.1090
39.32	188.0	26.6	1.94	21.469	.9903	-12.393	-.2871
39.32	183.9	26.0	1.94	20.599	.9714	-7.399	-.1752
48.41	185.9	26.2	1.94	20.899	.9753	-6.891	-.1616
48.41	186.6	26.4	1.94	21.469	.9974	-10.944	-.2554
58.67	186.3	26.2	1.94	20.889	.9740	-5.443	-.1275
58.67	187.2	26.5	1.94	21.469	.9937	-8.048	-.1871
69.67	190.3	26.8	1.94	22.049	1.0061	-7.033	-.1612
69.67	185.2	26.2	1.94	21.759	1.0187	-11.161	-.2625
90	183.5	26.0	1.93	21.179	.9997	-4.211	-.0998
STD	187.6	26.5	1.94	17.698	.8186	-9.579	-.2225
STD	183.8	26.0	1.94	17.407	.8212	-10.087	-.2390

Table A2 Reduced Data, Mach 2.88.

Θ (deg)	P_o (KP$_a$) abs	P_w (KP$_a$) abs	M_∞	$|X|$ (N)	C_{D_T}	M (N cm)	C_{M_T}
0	336.8	10.9	2.88	10.154	.5129	-.333	-.0085
0	340.2	11.1	2.88	10.154	.5070	-.333	-.0084
7.83	338.2	11.0	2.88	11.025	.5538	1.914	.0483
7.83	338.6	11.1	2.88	9.864	.4930	7.848	.1970
7.83	340.2	11.1	2.88	10.154	.5069	5.460	.1369
7.83	340.1	11.0	2.88	10.735	.5370	1.407	.0353
7.83	340.5	11.1	2.88	10.150	.5069	6.184	.1550
7.83	339.5	11.0	2.88	10.444	.5237	4.519	.1138
7.83	339.5	10.9	2.90	9.864	.4963	9.296	.2349
18.21	340.6	11.1	2.88	12.475	.6216	6.625	.1658
18.21	342.5	11.0	2.90	12.185	.6076	9.737	.2439
18.21	342.9	11.1	2.88	11.895	.5899	12.126	.3020
18.21	328.6	10.8	2.88	12.185	.6275	5.393	.1395
18.21	354.3	11.5	2.89	13.056	.6274	6.916	.1669
28.81	337.2	11.0	2.88	14.796	.7433	4.894	.1235
28.81	330.0	10.8	2.88	13.636	.7009	11.552	.2982
28.81	368.6	12.0	2.88	15.667	.7224	10.037	.2325
39.32	338.9	11.1	2.88	16.247	.8213	8.880	.2232
39.32	334.7	10.9	2.88	16.247	.8243	11.052	.2816
39.32	358.8	11.6	2.88	17.407	.8255	10.911	.2599
48.41	338.2	11.1	2.88	17.698	.8860	9.246	.2325
58.67	338.4	11.0	2.88	18.568	.9308	8.597	.2165
69.67	339.4	11.0	2.88	18.858	.9441	11.277	.2835
90	341.1	11.1	2.88	20.019	.9985	6.791	.1701
STD	339.7	11.0	2.88	13.056	.6534	1.124	.0282
STD	329.1	10.8	2.88	12.475	.6422	4.453	.1151
STD	354.2	11.4	2.89	13.056	.6298	4.020	.0974

Table A3 Reduced Data, Mach 4.0.

Θ (deg)	P_o (KPa)abs	P_w (KPa)abs	M_∞	$|X|$ (N)	C_{D_T}	M (N cm)	C_{M_T}
0	1,017.9	6.5	4.02	8.123	.3542	-6.059	-.1327
0	1,028.0	6.3	4.05	8.704	.3857	-10.122	-.2250
7.83	1,038.6	6.5	4.04	8.704	.3779	-9.388	-.2047
7.83	1,027.3	6.3	4.06	8.414	.3744	-6.999	-.1564
18.21	1,045.5	6.6	4.03	10.444	.4466	1.623	.0348
18.21	1,030.1	6.5	4.03	10.444	.4533	.899	.0196
28.81	1,024.8	5.5	4.03	12.765	.5552	3.512	.0767
28.81	1,027.3	6.4	4.04	12.475	.5456	5.901	.1296
39.32	1,034.9	6.6	4.03	15.377	.6617	5.185	.1121
39.32	1,028.0	6.4	4.04	15.086	.6618	6.125	.1350
48.41	1,034.2	6.6	4.03	16.827	.7249	7.723	.1671
48.41	1,031.5	6.4	4.04	17.117	.7475	4.611	.1011
58.67	1,033.5	6.6	4.02	19.438	.8349	.707	.0153
58.67	1,031.5	6.4	4.04	19.728	.8615	-1.681	-.0369
69.67	1,034.9	6.6	4.02	20.019	.8563	3.895	.0837
69.67	1,033.5	6.5	4.03	20.889	.9026	-1.823	-.0396
90	1,030.1	6.6	4.02	20.309	.8727	5.127	.1107
90	1,031.4	6.6	4.03	20.309	.8751	5.127	.1110
STD	1,034.5	5.5	4.04	11.315	.4903	-4.095	-.0891
STD	1,041.4	6.8	4.00	11.025	.4617	-.9821	-.0207

APPENDIX B

1. Loading with momoment only.

When the balance is loaded with a pure moment only, the axial load, X, is zero (see Fig. 9). Under these conditions Eq. (6) reduces to:

$$(C-D) = (A-B)$$

so that, from Eq. (8):

$$K = -\frac{(C-D)}{M} = -\frac{(A-B)}{M} \qquad [\frac{i.p.d.}{N\ cm}]$$

where i.p.d. = increments of pen deflection on the recording strip charts.

Data for the determination of K are illustrated in Fig. B1. The least quares fit of these data give:

$$K = -0.1381\ \frac{i.p.d.}{N\ cm}$$

2. Loading with axial force only.

When the balance is loaded under this condition, (see Fig. 8) Eqs. (6) and (8) reduce to the following forms:

$$c = K(\overline{y}_\ell - \overline{y}_u) = \frac{(C-D)-(A-B)}{X} \qquad [\frac{i.p.d.}{N}]$$

and

$$\frac{\overline{y}_\ell}{\overline{y}_u} = \frac{(C-D)}{(A-B)}$$

The constant c is determined by a least squares fit of the calibration data. These data are illustrated in Fig. B2. The result is:

$$c = -0.3447 \quad [\frac{i.p.d.}{N}]$$

Using the mean value for (C-D)/(A-B):

$$\frac{\bar{y}_\ell}{\bar{y}_u} = 1.4350$$

These results combined with the K value obtained from the moment calibration can be used to solve for the following mean effective gage locations:

$$\bar{y}_\ell - \bar{y}_u = \frac{c}{K} = 2.4957 \text{ cm}$$

$$\bar{y}_u = \frac{(\bar{y}_\ell - \bar{y}_u)}{(\frac{\bar{y}_\ell}{\bar{y}_u}) - 1} = 5.7373 \text{ cm}$$
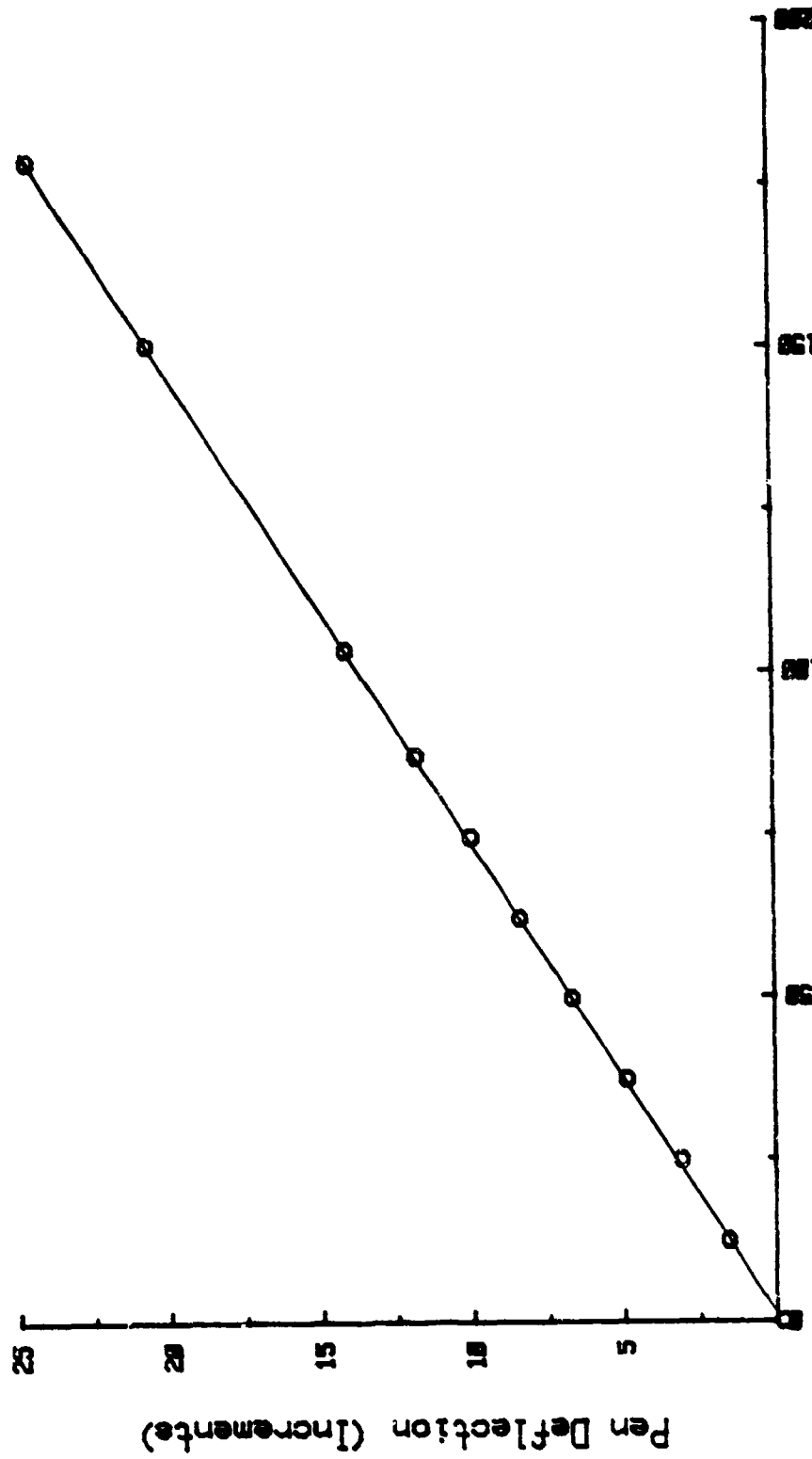
$$\bar{y}_\ell = \frac{(\bar{y}_\ell - \bar{y}_u)}{1 - (\frac{\bar{y}_u}{\bar{y}_\ell})} = 8.2331 \text{ cm}$$

Figure B1. Balance moment calibration, applied moment vs. increments of strip chart pen deflection.
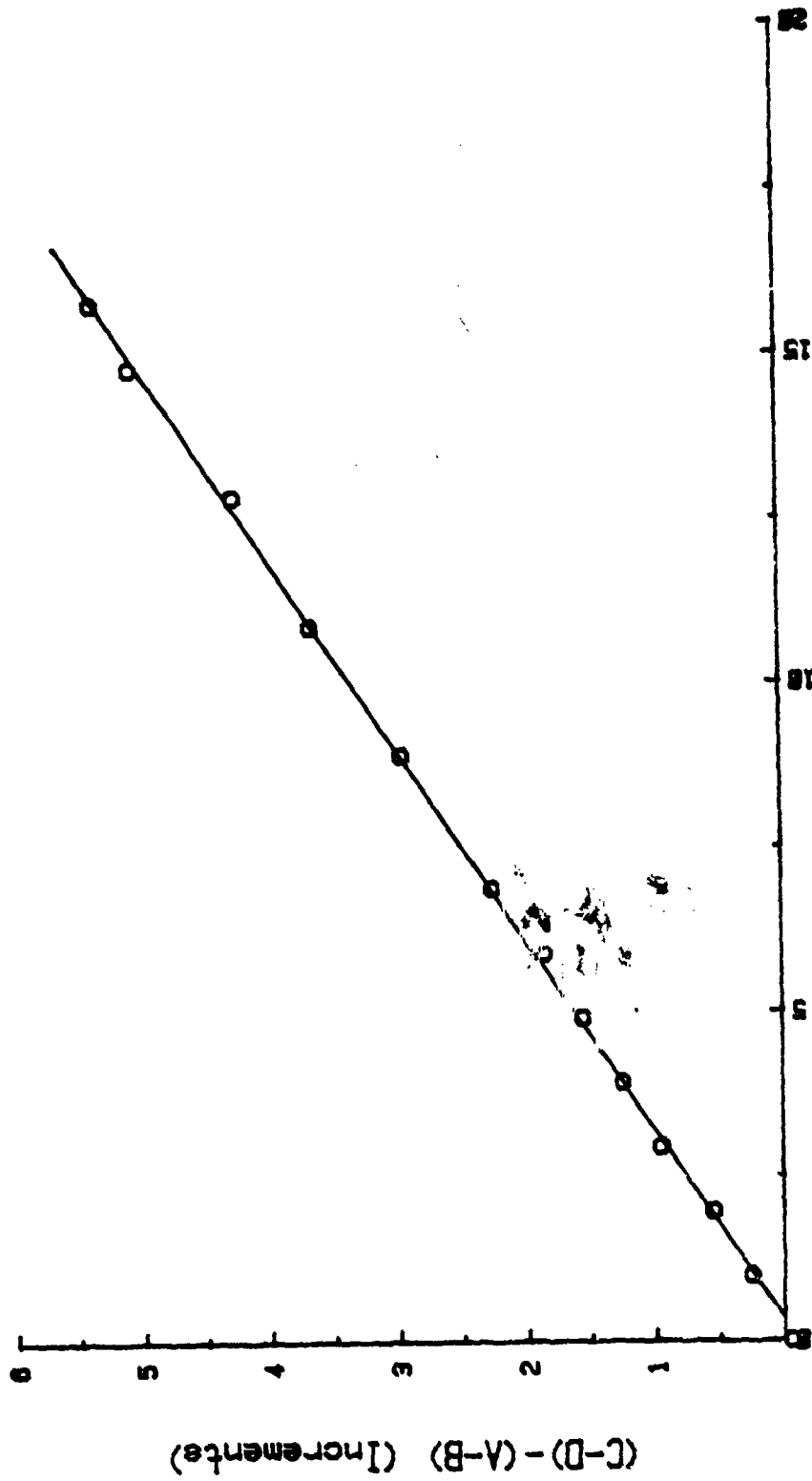
Figure B2. Balance drag calibration, applied axial force vs. increments of strip chart pen deflection.

65

LIST OF REFERENCES

1. Fackner, W. P., <u>Concept Evaluation of Tubular Round for Vulcan</u>, USARADBD-195. May 1978.

2. Vehicle Research Corporation Report No. 26, <u>High Performance Hollow Projectiles</u>, by Scott Rethorst, et. al., August 1973.

3. Air Force Armament Test Laboratory Technical Report 77-109, <u>Spinning Tubular Projectile Test Program</u>, by T. D. Kitchen and J. W. Keeser, Jr., September 1977.

4. Ballistic Research Laboratories Report, <u>Retardation of Tubular Projectiles Developed from the 20 MM American Ball</u>, by A. C. Charters, R. N. Thomas, Ordnance Center Project No. 3858, Aberdeen Proving Ground, Maryland.

5. Naval Postgraduate School Report 69-81-001, <u>Ball Motion in a Ball-Obturated Tubular Projectile</u>, by R. H. Nunn, J. W. Bloomer II, January 1981.

6. Bloomer, J. W. II, <u>Ball Obturation of a Spin Stabilized Tubular Projectile</u>, Machanical Engineers Thesis, Naval Postgraduate School, Monterey, California, June 1980.

7. Ballistic Research Laboratories Memorandum Report No. 2192, <u>Comparative Evaluation of the 20-mm Developmental Ammunition-Exterior Ballistics</u>, by Maynard J. Piddington, Aberdeen Proving Ground, Maryland.

8. Holman, J. P., <u>Experimental Methods for Engineers</u>, Third Edition, McGraw-Hill Book Company, 1978.

BIBLIOGRAPHY

Beckwith, T. G., Buck, N. Lewis, Mechanical Measurements, Addison-Wesley Publishing Company, Reading, Massachusetts, 1969.

John, James E. A., Gas Dynamics, Allyn and Bacon, Boston, Massachusetts, 1969.

Keenan, Joseph H. and Kaye, Joseph, Gas Tables, John Wiley and Sons, Inc., New York, 1945.

NACA Report 1135, Equations and Ch ts for Compressible Flow, Ames Research Laboratories, Moffett Field, California.

INITIAL DISTRIBUTION LIST

No. Copies

1. Defense Technical Information Center   2
   Cameron Station
   Alexandira, Virginia 22314

2. Library, Code 0142   2
   Naval Postgraduate School
   Monterey, California 93940

3. Department Chairman, Code 69Mx   2
   Department of Mechanical Engineering
   Naval Postgraduate School
   Monterey, California 93940

4. Professor R. H. Nunn, Code 69Nn   5
   Naval Postgraduate School
   Monterey, California 93940

5. LT William A. Bry, USN   1
   125 Fox Chase Lane
   Cherry Hill, New Jersey 08034